haematologica
Journal of The Ferrata Storti Foundation

The NADPH oxidase NOX2 is a marker of adverse prognosis involved in chemoresistance of acute myeloid leukemias

by Rosa Paolillo, Mathias Boulanger, Pierre Gâtel, Ludovic Gabellier, Marion De Toledo, Denis Tempé, Rawan Hallal, Dana Akl, Jérôme Moreaux, Hayeon Baik, Elise Gueret, Christian Recher, Jean-Emmanuel Sarry, Guillaume Cartron, Marc Piechaczyk and Guillaume Bossis

Received: August 27, 2021.
Accepted: February 8, 2022.

Citation: Rosa Paolillo, Mathias Boulanger, Pierre Gâtel, Ludovic Gabellier, Marion De Toledo, Denis Tempé, Rawan Hallal, Dana Akl, Jérôme Moreaux, Hayeon Baik, Elise Gueret, Christian Recher, Jean-Emmanuel Sarry, Guillaume Cartron, Marc Piechaczyk and Guillaume Bossis.The NADPH oxidase NOX2 is a marker of adverse prognosis involved in chemoresistance of acute myeloid leukemias.
Haematologica. 2022 Feb 17. doi: 10.3324/haematol.2021.279889. [Epub ahead of print]

The NADPH oxidase NOX2 is a marker of adverse prognosis involved in chemoresistance of acute myeloid leukemias

Rosa Paolillo[1,2], Mathias Boulanger[1,2], Pierre Gâtel[1,2,*], Ludovic Gabellier[1,2,3,*], Marion De Toledo[1,2], Denis Tempé[1,2], Rawan Hallal[1,2], Dana Akl[1,2], Jérôme Moreaux[4], Hayeon Baik[1,2], Elise Gueret[5], Christian Recher[6,7], Jean-Emmanuel Sarry[7], Guillaume Cartron[3], Marc Piechaczyk[1,2] and Guillaume Bossis[1,2]

Affiliations:

1- IGMM, Univ Montpellier, CNRS, Montpellier, France

2- Equipe labellisée Ligue Contre le Cancer, Paris, France

3- Département d'Hématologie Clinique, CHU de Montpellier, Montpellier, France

4- IGH, Univ Montpellier, CNRS, Montpellier, France

5- MGX, Univ Montpellier, CNRS, INSERM, Montpellier, France

6- Service d'Hématologie, CHU de Toulouse, Toulouse, France

7- CRCT, University of Toulouse, INSERM, CNRS, Toulouse, France

Running title : NOX2 is involved in AML chemoresistance

Correspondence to:

guillaume.bossis@igmm.cnrs.fr

Phone: 0033434359664

Fax: 0033434359634

* equal contribution

The authors declare no potential conflict of interest related to this work

Acknowledgments

We are grateful to the IGMM "Ubiquitin Family in Hematological Malignancies" group members for fruitful discussions and critical reading of the manuscript. We thank the Montpellier Ressources Imagerie (MRI) platforms for technical assistance. Funding was provided by the CNRS, the Fondation ARC pour la recherche sur le cancer, Ligue Nationale contre le Cancer (Programme Equipe Labellisée), the INCA (ROSAML), the ANR ("Investissements d'avenir" program; ANR-16-IDEX-0006), the Fondation pour la Recherche Médicale (FRM) to LG and the Ligue Nationale contre le Cancer to MB. The HEMODIAG_2020 collection of clinical data and patient samples was funded by the Montpellier University Hospital, the Montpellier SIRIC and the Languedoc-Roussillon Region. MGX acknowledges financial support from the France Génomique National infrastructure, funded as part of "Investissements d'Avenir" program managed by the Agence Nationale pour la Recherche (contract ANR-10-INBS-09).

Disclosures

CR received research funding from AbbVie, Amgen, Novartis, Celgene, Jazz Pharmaceuticals, Agios, Chugai, MaatPharma, Astellas, Roche, Iqvia, Daiichi-Sankyo and did consultancy/advisory role for AbbVie, Janssen, Jazz Pharmaceuticals, Novartis, Celgene, Otsuka, Astellas, Daiichi-Sankyo, Macrogenics, Roche, Takeda, and Pfizer.

GC did consulting for Roche, Celgene, MabQi, MedXcell and receive honoraria from Abbvie, Janssen, Novartis, Milteny, Roche, Gilead.

Contributions

RP, PG, MdT, RH, DA, HB performed the cell biology experiments and analyzed the data. MB and DT analyzed the RNA-Seq data. LG and JM created and validated the NOX prognosis score. EG performed the sequencing of the RNA-Seq. GC provided patient samples. CR, JS, MP and GB designed the study and obtained funds for the project. GB supervised the study.

Data sharing statement

Sequencing data were deposited on Gene Expression Omnibus with accession number GSE193094.

Abstract

Resistance to chemotherapeutic drugs is a major cause of treatment failure in Acute Myeloid Leukemias (AML). To better characterize the mechanisms of chemoresistance, we first identified genes whose expression is dysregulated in AML cells resistant to daunorubicin (DNR) or cytarabine (Ara-C), the main drugs used for the induction therapy. The genes found activated are mostly linked to immune signaling and inflammation. Among them, we identified a strong up-regulation of the NOX2 NAPDH oxidase subunit genes (*CYBB*, *CYBA*, *NCF1*, *NCF2*, *NCF4* and *RAC2*). The ensuing increase in NADPH oxidase expression and ROS production, which is particularly strong in DNR-resistant cells, participates in the acquisition and/or maintenance of resistance to DNR. $Gp91^{phox}$ (*CYBB*-encoded Nox2 catalytic sub-unit), was found more expressed and active in leukemic cells from the FAB M4/M5 subtypes patients compared to FAB M0-M2 ones. Moreover, its expression was increased at the surface of patient's chemotherapy resistant AML cells. Using a gene expression-based score we finally demonstrate that high NOX2 subunit genes expression is a marker of adverse prognosis in AML patients. The prognosis NOX score we defined is independent of the cytogenetic-based risk classification, FAB subtype, FLT3/NPM1 mutational status and age.

Introduction

Acute Myeloid Leukemias (AML) are a heterogeneous group of hematological malignancies resulting from the transformation of hematopoietic stem- or progenitor cells. Prognosis is poor, in particular for old patients (>60 years)[1]. For fit patients, the standard treatment generally relies on intensive chemotherapy combining 3 days of an anthracycline (daunorubicine-DNR or idarubicine-IDA) and 7 days of cytarabine (Ara-C) ("3+7" regimen)[2]. Resistance to chemotherapy remains the main cause of relapse and death. However, the mechanisms responsible for chemoresistance acquisition and maintenance are not fully elucidated. Among those described are changes in the drug uptake/efflux[3], modulation of the pro-drug activation process[4,5], higher resistance to apoptosis[6], enhanced DNA repair abilities[7] and modulations of energetic and redox metabolisms[8,9]. A better characterization of the pathways dysregulated in chemoresistant AML would be instrumental to find new therapeutic targets to overcome chemoresistance. This could also provide new biomarkers allowing improvement of AML risk stratification, which is currently mostly based on the number and nature of the cytogenetic abnormalities[2]. Such prognosis biomarkers might help clinicians in their therapeutic decision. This is all the more to be considered as new therapies, such as those targeting mutated FLT3 and IDH1/2 or BCL2, are emerging as promising alternative to standard chemotherapies[10].

Here, we have addressed the mechanisms underlying AML resistance through the identification of genes whose expression is dysregulated in AML cells resistant to DNR or Ara-C. We found that chemoresistant AML cells mostly activate genes related to inflammatory response. In particular, we identified a strong up-regulation of the different subunits of the NADPH oxidase NOX2. NADPH oxidases constitute a seven members family of multi-subunit oxidases, whose sole function is the production of ROS[11]. NOX2 is the main NOX isoform expressed in myeloid cells and was found overexpressed in AML[12]. In line with their overexpression, we found a large increase in NOX-derived ROS production in chemoresistant AML cells, particularly in those resistant to DNR. This activation of NOX2 and the subsequent increase in ROS production participates in the acquisition/maintenance of the resistant phenotype. In addition, we found that NOX2 expression increases at the surface of chemotherapy-resistant AML blasts. Finally, we provide evidence that NOX2 is a marker of both chemoresistance and adverse prognosis in AML patients.

Methods

Additional methods can be found as supplementary material.

Patient samples

Bone marrow aspirates were collected at diagnosis or after induction chemotherapy (15 to 45 days after the beginning of the chemotherapeutic regimen comprising a combination of DNR and Ara-C). Written informed consent was obtained from patients after approval by the institutional "Sud Méditerranée 1" Ethical Committee (ref 2013-A00260-45; HemoDiag collection). Immediately after collection, leukocytes were purified by density-based centrifugation using Histopaque 1077 (Sigma-Aldrich) and used for flow cytometry analysis. Clinical characteristics of the patients are provided in Supplementary Table 3. When indicated, cells were sorted after CD45/SSC gating[13] with a CD45-Pacific-Blue antibody (Beckman Coulter) and CD34-PerCP-Vio700 (Miltenyi Biotec) using an Aria IIU cell sorter (Becton Dickinson).

Flow cytometry

Cells were washed in PBS containing 2% FBS and incubated at 4°C for 30 minutes in the presence of FITC-conjugated $gp91^{phox}$ antibodies (D162-4; MBL), washed and analyzed using LSR Fortessa flow cytometer (Becton Dickinson). For patient samples, leukemic cells were identified using CD45/SSC gating[13] (see Supplementary Figure 6 for a gating example). The median fluorescence intensities for $gp91^{phox}$ on the red blood cells present in the samples (negative control) was subtracted from the mean fluorescence intensities for $gp91^{phox}$ on the leukemic cells.

RNA-seq libraries preparation and sequencing

Total RNAs were purified using the GenElute Mammalian Total RNA kit (Sigma-Aldrich), treated with DNase I (4U, New England Biolabs) and RNasin (2.5U, Promega) and re-purified. RNA quality was assessed using a BioAnalyzer Nano 6000 chip (Agilent). Three independent experiments were performed for each cell line. Libraries were prepared using TruSeq®Stranded mRNA Sample Preparation kit (Illumina). Libraries were sequenced using an Illumina Hiseq 2500 sequencer as single-end 125 base reads. Image analysis and base calling were performed using HiSeq Control Software (HCS), Real-Time Analysis (RTA) and bcl2fastq. The RNA-Seq sequencing data are available on the Gene Expression Omnibus repository under accession number GSE193094

Generation of a prognosis score based on the expression of NOX2 genes

Gene expression data from three independent cohorts of adult patients diagnosed with AML were used[14–16]. Patients without available survival data, with myelodysplastic syndrome diagnosis or not treated with conventional chemotherapy were excluded. The first cohort (Verhaak cohort)[15] included 504 patients. The second (Metzeler cohort)[16] comprised 242 patients with normal karyotype (CN-AML). The third (TCGA)[14] included 148 patients. Gene Expression Omnibus accession numbers are GSE6891, GSE12417 and GSE68833. *FLT3/NPM1* statuses for the Metzeler cohort patients were kindly provided by Metzeler et *al.*[16]. Because data normalization was different, expression level was normalized using standard normal cumulative distribution ($X' = (X-\mu)/\sigma$) for each gene. In the first cohort, cutpoints were determined for the 6 genes of interest (*CYBA, CYBB, NCF1, NCF2, NCF4, RAC2*) using MaxStat analysis, therefore defining beta coefficients. The first cohort was then randomly divided in two sub-cohorts of 252 patients each (training and test sets). As previously described[17–20], we created a gene expression-based risk score based on the levels of expression of all NOX2 constituent genes in the training set. It was defined for each patient as the sum of the beta coefficients for all these genes weighted by +1 or -1 according to the patient sample signal above or below/equal the probeset MaxStat value. Thus, overexpression of genes associated with a poor prognosis increased the NOX score while overexpression of those associated with a good prognosis decreased it. Patients from the training cohort were ranked according to increased NOX score and, for a given score value Y, the difference in survival of patients with a NOX score $\leq Y$ or $>Y$ was computed using MaxStat. The NOX score was then individually computed for patients in the test set, using the cutoff value determined in the training cohort. Finally, we transposed our model in the validation cohorts (Metzeler and TCGA cohort), using both cutpoints defined for each probeset and the cutoff score determined in the training set. Survival analyses were assessed using Kaplan-Meier method and survival curves were compared using log-rank test. Univariate and multivariate analysis was performed using the Cox proportional hazard model.

Results

Chemoresistant AML cells activate inflammation-related transcriptional programs.

To study AML chemoresistance, we performed RNA-Seq in the AML model cell line HL-60, using parental cells and DNR-resistant (DNR-R) or Ara-C-resistant (ARA-R) cell populations[21]. We identified 989 differentially expressed genes between drug-resistant and parental HL-60 cells (Figures 1A and Supplementary Table 1). Among them, some were up-regulated in resistant cells (452 for DNR-R and 283 for ARA-R) and others were down-regulated (312 for DNR-R and 146 for ARA-R). 132 genes were commonly up-regulated and 38 down-regulated in both types of resistant cells compared to parental cells (Figure 1A). In general, the most deregulated genes showed the same trend of up- or down-expression in both DNR-R and ARA-R cells (Figures 1B and 1C). However, many genes were preferentially modulated upon acquisition of resistance to one of the two drugs (594/764 for DNR-R and 259/429 for ARA-R) (Figures 1A and Supplementary Figure 1A).

Ontological analysis of the genes up-regulated in both ARA-R and DNR-R cells showed a strong enrichment for immune signaling and inflammation (Figure 1D). An enrichment of few pathways involved in the regulation of transcription was found for the genes down-regulated in DNR-R cells, and no enrichment for specific pathways was found for the genes down-regulated in ARA-R cells (Supplementary Table 2). Gene set enrichment analysis (GSEA) further showed an enrichment of an inflammatory signature for the genes up-regulated in resistant *versus* parental HL-60 cells (Figure 1E). This signature included various cytokines and chemokines, which are up-regulated in both types of resistant cells, with, however, stronger induction in DNR-R cells (Supplementary Figure 1B).

We then wondered if the inflammatory signature could also be enriched in patients relapsing after chemotherapy. We thus used publicly available transcriptomic data obtained from 9 patients at diagnosis and relapse[22]. A GSEA analysis revealed that the inflammatory signature was enriched at relapse, in the 3 patients from the FAB M2 subtype (Figure 1F) but not in those from the M1 and M4 subtypes (Supplementary Figure 2A and 2B). Accordingly, a signature containing all genes up-regulated in both ARA-R and DNR-R HL-60 cells was found enriched at relapse in M2 patients but not in M1 and M4 patients (Supplementary Figure 2C), suggesting that the mechanisms underlying chemoresistance differ depending of the degree of maturation of the leukemic clone. Finally, the genes up-regulated specifically in DNR-R cells were also enriched in genes involved in inflammation whilst those enriched only in ARA-R cells were not enriched for any specific pathway (Supplementary Table 2). Thus,

our data suggest that AML resistance to chemotherapies, in particular DNR, can be associated with transcriptional reprogramming involving the induction of an inflammatory response.

Resistance to DNR is associated with strong overexpression and activation of the NAPDH oxidase NOX2.

At the top of the list of genes up-regulated in the inflammatory response signature of resistant cells, in particular those resistant to DNR, we identified *CYBB* (Supplementary Figure 1B). It encodes the $gp91^{phox}$ protein, the catalytic subunit of NOX2, the NADPH oxidase (NOX) family member principally expressed in the hematopoietic system and in AML[23]. Two of the NOX2 subunits, $gp91^{phox}$ and $p22^{phox}$ are associated with the plasma membrane (Figure 2A). Upon activation, the cytosolic subunits ($p67^{phox}$, $p47^{phox}$ and $p40^{phox}$) and the small GTPase Rac2 are recruited to the membrane and activate the oxidase[24]. This leads to the production of extracellular superoxides, which can freely diffuse across the plasma membrane.

Further pointing to a link between NOX2 and DNR resistance, a NADPH oxidase signature was found to be enriched in DNR-R cells compared to parental cells (Supplementary Figure 2D). Indeed, although *CYBB* was found up-regulated in both ARA-R and DNR-R cells, the other NOX2 subunits were specifically up-regulated in DNR-R as compared to parental HL-60 cells (Figure 2B). RT-qPCR analysis confirmed that *CYBB* is strongly up-regulated in DNR-R cells and, to a lower extent, in ARA-R cells, as compared to parental HL-60 cells (Figure 2C). The *NCF2* gene (encoding $p67^{phox}$) was also overexpressed in DNR-R but not in ARA-R cells (Figure 2C). To assess whether higher gene expression translates into higher NADPH oxidase activity, we measured extracellularly-produced superoxides ($^{\cdot}O_2$-). Basal NADPH oxidase activity is low under standard growth conditions because the cytosolic subunits are not bound to the membrane. We therefore treated cells with PMA, a well-known activator of NADPH oxidases. No superoxide production was detected in HL-60 cells, which are known to have a low/absent NADPH oxidase activity when not differentiated[25,26]. A strong ROS production was measured in PMA-treated DNR-R but not in ARA-R cells (Figure 2D). To confirm these results, we used another cell line, U937, rendered resistant to Ara-C or DNR[21]. DNR- but not Ara-C-resistant U937 cells had increased NOX activity (Figure 2E), overexpressed CYBB and NCF2 and expressed higher levels of $gp91^{phox}$ at their surface compared to parental cells (Figure 2F).

We then cloned the chemoresistant HL-60 cell populations. All DNR-R clones showed a strong increase in both *CYBB* (Figure 3A) and *NCF2* (Figure 3B) mRNA levels (above 10 to

more than 1000-fold compared to HL-60 cells). Accordingly, PMA-induced extracellular ROS production was increased in all DNR-R clones compared to parental HL-60 (Figure 3C). Although the Ara-C-resistant population showed no significant increase in ROS production (Figure 2E), a fraction of the ARA-R clones showed an increase in *CYBB* and *NCF2* expression and high NOX activity in comparison to parental HL-60 cells (Figure 3A, 3B and 3C). The mean increase in NOX activity was however around 7-fold lower in ARA-R- compared to DNR-R clones, which might explain why it was not detected within the ARA-R resistant population. In addition, ARA-R clones with high NOX activity might have a survival advantage of the during the cloning process. To exclude the possibility that increased NOX2 expression and activity was due to the cloning procedure, we cloned the parental HL-60 cells. None of the HL-60 clones showed an increase in NADPH oxidase-derived ROS production (Supplementary Figure 3). To determine if high NOX activity was sufficient to confer DNR resistance, we measured the IC50 for DNR of two ARA-R clones, one with low NOX activity (15138) and one with high NOX activity (15144). None of the ARA-R clone were resistant to DNR, indicating that high NOX expression in ARA-R cells is not sufficient to confer cross-resistance to DNR (Supplementary Figure 4A). In addition, higher NOX activity was not conferring resistance to Venetoclax, a BCL2 inhibitors now used in AML patients' treatment (Supplementary Figure 4B). Finally, for both DNR-R and ARA-R clones, increased NOX activity was not correlated with a significant increase in the differentiation of the chemoresistant clones (Supplementary Figure 4C).

We then measured $gp91^{phox}$ membrane expression using flow cytometry of two high ROS-producing clones (15165 and 15176) and two low ROS-producing clones (15160 and 15169) from DNR-R cells. Overexpression of $gp91^{phox}$ at the cell surface was found to be high only in the clones producing high levels of ROS (15165 and 15176) (Figure 3D). VAS2870, a pan-NADPH oxidase inhibitor with preferential activity against NOX2[27], strongly reduced PMA-induced ROS production in DNR-R clones (Figure 3E), further demonstrating that increased ROS production in chemoresistant AML cells is due to NADPH oxidase activation.

Altogether, our data suggest that acquisition of chemoresistance, in particular to DNR, is associated with increased expression of the subunits of the NOX2 NADPH oxidase, its cell surface expression and activity in AML cells.

$gp91^{phox}$ overexpression does not affect chemoresistant cells proliferation but participates in their resistance to DNR.

To address the role of NOX2 activation in chemoresistant cells, we measured the proliferation of 4 DNR-R and 2 ARA-R clones (one high and one low NOX2 expressing clone). No differences were observed in their proliferation compared to parental HL-60 cells (Supplementary Figure 4D), suggesting that high NOX2 is not conferring a proliferative advantage to the chemoresistant cells. Then, using the CRISPR/Cas9 technology, we knocked out the *CYBB* gene in the DNR-R clone showing the highest level of $gp91^{phox}$ expression (clone 15165). This led to a strong decrease in $gp91^{phox}$ cell surface expression (Figure 4A) and abolished NADPH oxidase activity (Figure 4B). No difference was observed between the proliferation rates of parental HL-60 and DNR-R cells expressing or not $gp91^{phox}$ (Figure 4C). DNR-R cells CRISPRed for $gp91^{phox}$ regained sensitivity to DNR compared to control CRISPRed cells (Figure 4D and Supplementary Figure 5C).

To further demonstrate the involvement of NOX2-derived ROS production in DNR resistance maintenance, we cultured for three weeks the parental HL-60 cells and two DNR-R clones (15165 and 15176) in medium supplemented with Superoxide Dismutase (SOD), which transforms superoxide anions to H_2O_2 and Catalase, which degrades H_2O_2 to H_2O[28,29]. This efficiently removed NOX2-produced ROS from the medium (Supplementary Figure 5A and 5B). Although this did not affect the proliferation of the DNR-R clones (Figure 4E), this decreased their resistance to DNR (Figure 4F). Similarly, long-term treatment of the DNR-R clones with the NOX inhibitor VAS2870 re-sensitized them to DNR (Supplementary Figure 5D). Altogether, this suggests that over-expression of $gp91^{phox}$ and the ensuing increase in ROS production contributes to the acquisition and/or the maintenance of resistance to DNR in our model.

$gp91^{phox}$ expression and NOX2 activity are higher in FAB M4/M5 AML subtypes and increase on chemotherapy-resistant AML patient's cells.

To further characterize the importance of NOX2 in AML patients, we flow cytometry-assayed the expression of $gp91^{phox}$ on the surface of primary AML cells from 74 patients at diagnosis. Differences in $gp91^{phox}$ levels were neither associated with a specific group from the ELN-2017 classification[2] (favorable, intermediate or adverse), nor with the NPM1 or FLT3 mutational status (Supplementary Figure 7 and Supplementary Table 3). However, $gp91^{phox}$ levels were significantly higher in the M5 AML subtypes compared to normal $CD34^+$ cells and leukemic blasts from the M0, M1 and M2 subtypes from the French-American British (FAB) classification (Figure 5A and Supplementary Table 3). Using transcriptomic data from

the TCGA cohort[14], we confirmed that *CYBB* mRNA expression is higher in the M4/M5 subtypes (Figure 5B). To assess whether increased gp91^{phox} cell surface expression is linked to higher NAPDH oxidase activity, we measured PMA-stimulated ROS production using sorted AML cells (bulk CD34$^-$ leukemic cells and Leukemic Stem Cells (LSC)- containing CD34$^+$ cells) from one patient with low gp91^{phox} (M1 subtype, patient #17215) and another with a high gp91^{phox} cell surface expression (M4 subtype, patient #17226) (Figure 5C). Weak PMA-induced ROS production was detected in the low gp91^{phox}-expressing patient cells, which contrasted with high production in high gp91^{phox}-expressing patient cells (Figure 5D). For the M4 patient cells, gp91^{phox} level (Figure 5C) and ROS production (Figure 5D) were much higher in the bulk of leukemic cells (CD34$^-$) than in the LSC-containing compartment (CD34$^+$).

Finally, for 8 patients or our cohort, we compared the mean gp91^{phox} expression on leukemic blasts taken at diagnosis with that on blasts that resisted induction therapy in the same patients. An increase in gp91^{phox} labelling after chemotherapy was found in 7 out 8 patients (Figure 5E and Supplementary Table 3). This supported the idea that, similarly to the chemoresistant cell lines, chemotherapy-resistant AML cells generally express higher levels of gp91^{phox} at their surface.

NOX2 overexpression is a marker of adverse prognosis in AML.

To study the link between NOX2 and AML response to treatments, we determined the individual prognosis value of the genes coding for the six NOX2 subunits (*CYBB*, *CYBA*, *NCF1*, *NCF2*, *NCF4*, *RAC2*) using publicly available data from the Verhaak cohort[15]. Increased expression was associated with a poor prognosis for four of them (*CYBB*, *NCF2*, *NCF4*, *RAC2*) and with a good prognosis for the other two (*CYBA* and *NCF1*) (Table 1). To take into account the expression and prognosis value of all NOX2 subunits instead of individual ones, we developed a NOX2 subunits gene expression-based score. The contribution of individual NOX2 genes and the cutpoint were determined using a training cohort comprising 252 patients (Verhaak training set)[15]. Patients with a high "NOX score" had a worse prognosis with a hazard ratio of 1.85 in univariate Cox analysis (Figure 6A and Table 2).

The prognosis significance of the NOX score was then confirmed in a test set (n=252) from the Verhaak cohort (Figure 6B and Table 2) as well as in two independent validation cohort: the Metzeler- [16] (Figure 6C, Table 2 and Supplementary Table 4) and the TCGA cohort[14]

(Figure 6D, Table 2 and Supplementary Table 6). The poor prognostic-based NOX score remained statistically significant in a multivariate Cox analysis including the cytogenetic-based classification, the NPM1/FLT3 mutational status (for the normal karyotype cohort), and age (Table 2). The NOX score strongly correlated with the expression of subunits associated with poor prognosis (*CYBB*, *NCF2*, *NCF4* and *RAC2*) while the correlation with *CYBA* and *NCF1* was less significant (Supplementary Figure 8). Finally, in line with the higher expression of *CYBB* in M4/M5 FAB subtypes, the NOX score was generally higher in the M4/M5 compared to the other FAB subtypes (Supplementary Figure 9). Nevertheless, the prognosis value of the NOX score was independent from the FAB subtype, which did not have prognostic value on its own in any of the cohorts (Table 2).

To determine if the worse prognosis of high NOX score patients could be associated to higher chemoresistance, we selected the 10% of patients with the highest NOX score and compared their transcriptome to those of the 50% of patients with the lowest NOX scores. We then used the 50 most up-regulated genes in the high NOX score patients (Supplementary Table 4) as a gene-set in a GSEA analysis of the RNA-Seq data from parental and chemoresistant HL-60 cells. The high NOX score gene set was significantly enriched in the chemoresistant compared to parental HL-60 cells (Figure 6E). Interestingly, the most up-regulated gene in the high NOX score patients is *NAMPT*, encoding a critical enzyme in the recycling of NAD, an essential co-factor for NADPH oxidase activity. Accordingly, we found that *NAMPT* expression is highly correlated to that of the *CYBB*, *NCF1* and *NCF2* genes in AML patients (Figure 6F).

Altogether, these data suggested that the overexpression of the NOX2 NADPH oxidase is a marker of adverse prognosis in AML associated with enhanced chemoresistance of the leukemic cells.

Discussion

Our work unveiled that NOX2 expression increases in chemoresistant AML and could participate to the acquisition/maintenance of chemoresistance. Moreover, NOX2 was found to be a marker of adverse prognosis in AML patients. NOX2 is the main NADPH oxidase complex expressed in the hematopoietic system. It is responsible for the respiratory burst, a release of superoxides ($^{\cdot}O_2^-$) in the phagosome, which is used to eliminate engulfed pathogens[30]. In addition to their essential role in host protection, ROS produced by NADPH oxidases also function as second messengers in the regulation of numerous signaling pathways[31]. Dysregulations of NADPH oxidases expression and activity have been linked to various cancers, including AML[32]. NOX2 expression was found to be generally higher in leukemic blasts from AML patients compared to normal $CD34^+$ hematopoietic progenitors and involved in leukemic cells proliferation[12]. NOX2 was shown to be mostly expressed in M4 and M5 subtypes of the FAB classification and rarely on leukemic blasts from M1 or M2 subtypes[26,33]. By analyzing the $gp91^{phox}$, the catalytic subunit of NOX2, at the surface of blasts from 74 AML patients, we confirmed that NOX2 expression is higher in the M4/M5 subtypes than in the M0, M1 and M2 subtypes. In addition, within a given patient sample, $gp91^{phox}$ expression and NOX2 activity were higher in the bulk of leukemic cells ($CD34^-$) compared to the LSC-containing $CD34^+$ compartment, which nevertheless showed basal activity. This is coherent with the fact that NOX2 is required for LSC self-renewal and, in turn, leukemogenesis[23]. Moreover, our results indicate that the increase in NOX2 activity in chemoresistant cell lines is linked with the transcriptional activation of most, if not all, of its six subunits. Interestingly, their expression, in particular those of *CYBB*, *NCF1* and *NCF2*, is highly correlated.

Increased NOX2 expression could confer a selective advantage to the chemoresistant clones. Supporting this hypothesis, we could demonstrate, in patients, that therapy resistant cells remaining after induction chemotherapy express higher levels of $gp91^{phox}$ at their surface. Moreover, preventing NOX2 activation in DNR-R cells through the deletion of *CYBB*, ROS scavenging or NADPH oxidase inhibition re-sensitized them to DNR. This indicates that NOX2 overexpression could be involved in the acquisition and/or maintenance of resistance. The underlying molecular mechanisms remain to be characterized. They might involve the regulation of specific signaling pathways through the reversible oxidation of cysteines present in the catalytic site of enzymes such as kinases and phosphatases[34] or, as we showed previously, of SUMOylation enzymes[35,36]. Their modulation would participate in the

transcriptional reprogramming observed in chemoresistant AML cells and in the acquisition and/or maintenance of chemoresistance. NOX-derived ROS were also shown to promote AML cell proliferation[12,37], possibly by activating genes involved in glycolysis[38] or through a metabolic reprograming[39]. In addition, oncogenes such as mutated *RAS*[40,41] or *FLT3-ITD*[42] activate NADPH-oxidase-derived ROS production, which increases hematopoietic cell proliferation and leukemic transformation. Finally, NOX2-derived ROS stimulate the transfer of mitochondria from bone marrow stromal cells to the AML blasts, increasing their metabolic activity and proliferation[43]. In our study, high NOX-expressing chemoresistant clones did not proliferate faster than chemosensitive parental cells and deletion of *CYBB* or ROS scavenging did not affect their doubling time. Thus, although the pro-proliferative effect of NOX-derived ROS might be involved in leukemogenesis, it does not seem to confer a proliferative advantage to chemoresistant cells. Finally, NADPH-oxidase derived ROS are also involved in the interaction between leukemic cells and the immune system. They can induce apoptosis of Natural Killers and T-cells[33] and prevent the maturation of Dendritic Cells[44]. Whether such an inactivation of anti-tumor immune cells could also confer a selective advantage to the chemoresistant AML cells that overexpress NOX2 remains an open question. When analyzing the prognosis value of the individual NOX2 subunits, we found that four were associated with a poor prognosis (gp91phox, p67phox, p40phox and Rac2) and, more surprisingly, two with a good prognosis (p22phox and p47phox). The association of *CYBA* (p22phox) and *NCF1* (p47phox) with a good prognosis might be due to NOX2 independent functions of these proteins. In particular, p22phox is also involved in the assembly of NOX1, NOX3 and NOX4[11] and p47phox can activate both NOX1[45] and NOX3[46]. We thus developed the NOX score to take into account the expression and the prognosis value of all subunits. Patients with a high NOX score showed overexpression of *CYBB*, *NCF2*, *NCF4* or *RAC2*. A high NOX score was associated with a poor prognosis in 3 independent AML cohorts. The NOX score was found to be independent from other prognosis factors such as age, cytogenetic risk or *NPM1/FLT3* mutational status in normal karyotype AML. Consistent with a higher expression of *CYBB* in FAB M4/M5 subtypes, we found that the NOX score was higher in these subtypes. However, the NOX score was found to be independent of the FAB classification in the multivariate analysis, indicating that its prognosis value is not linked to the FAB subtype. Although patient with high NOX score showed enrichment in the signature of chemoresistance, the prognosis value of the NOX score might not only be linked to the role of NOX2 on chemoresistance. The NOX score should now be validated in a prospective cohort to confirm its prognosis value. NAPDH-oxidase inhibitors have been proposed as

anti-cancer drugs. Histamine, which inhibits NADPH-oxidase-derived ROS production, is already approved, in combination with IL-2, to prevent relapse in AML[47]. This treatment was found to be more effective in M4/M5 patients[48]. The NOX score might constitute another biomarker to select patients eligible for such therapy. Many other molecules targeting NADPH oxidases have been developed in the past few years[49]. However, most of them suffer from a lack of specificity[50,51]. Interestingly, we found that NAMPT, a rate-limiting enzyme in the recycling of NAD, is the most upregulated gene in the high NOX score patients and its expression is highly correlated to NOX2 subunits levels in AML patients. In addition, NAMPT was more expressed in chemoresistant HL-60 cells than in parental cells, in line with recent findings showing its overexpression in chemoresistant *versus* chemosensitive LSC[52]. Inhibitors of NAMPT have shown anti-leukemic activity in preclinical models[52–54] and some of them are being tested in clinical trials (NCT02702492, NCT04281420). Even though the NADP/NADPH cycle relies on various enzymatic activities, targeting NAMPT in high NOX score-expressing patients might therefore represent another option to inhibit NOX2 activity in AML cells, by decreasing NADPH supply. Altogether, our work points to a link between NOX2 and AML chemoresistance. Its targeting might constitute a new therapeutic strategy to overcome AML chemoresistance and improve their prognosis.

References

1. Döhner H, Weisdorf DJ, Bloomfield CD. Acute Myeloid Leukemia. N Engl J Med. 2015;373(12):1136-1152.
2. Döhner H, Estey E, Grimwade D, et al. Diagnosis and management of AML in adults: 2017 ELN recommendations from an international expert panel. Blood. 2017;129(4):424-447.
3. Marin JJG, Briz O, Rodríguez-Macias G, Díez-Martín JL, Macias RIR. Role of drug transport and metabolism in the chemoresistance of acute myeloid leukemia. Blood Rev. 2016;30(1):55-64.
4. Galmarini CM, Thomas X, Graham K, et al. Deoxycytidine kinase and cN-II nucleotidase expression in blast cells predict survival in acute myeloid leukaemia patients treated with cytarabine. Br J Haematol. 2003;122(1):53-60.
5. Ax W, Soldan M, Koch L, Maser E. Development of daunorubicin resistance in tumour cells by induction of carbonyl reduction. Biochem Pharmacol. 2000;59(3):293-300.
6. Sillar JR, Enjeti AK. Targeting Apoptotic Pathways in Acute Myeloid Leukaemia. Cancers (Basel). 2019;11(11):1660.
7. Pearsall EA, Lincz LF, Skelding KA. The Role of DNA Repair Pathways in AML Chemosensitivity. Curr Drug Targets. 2018;19(10):1205-1219.
8. Hosseini M, Rezvani H, Aroua N, et al. Targeting Myeloperoxidase Disrupts Mitochondrial Redox Balance and Overcomes Cytarabine Resistance in Human Acute Myeloid Leukemia. Cancer Res. 2019;79(20):5191-5203.
9. Farge T, Saland E, Toni F de, et al. Chemotherapy Resistant Human Acute Myeloid Leukemia Cells are Not Enriched for Leukemic Stem Cells but Require Oxidative Metabolism. Cancer Discov. 2017;7(7):716-735.
10. Fiorentini A, Capelli D, Saraceni F, Menotti D, Poloni A, Olivieri A. The Time Has Come for Targeted Therapies for AML: Lights and Shadows. Oncol Ther. 2020;8(1):13-32.
11. Moghadam ZM, Henneke P, Kolter J. From Flies to Men: ROS and the NADPH Oxidase in Phagocytes. Front Cell Dev Biol. 2021;9:628991.
12. Hole PS, Zabkiewicz J, Munje C, et al. Overproduction of NOX-derived ROS in AML promotes proliferation and is associated with defective oxidative stress signaling. Blood. 2013;122(19):3322-3330.
13. Brahimi M, Saidi D, Touhami H, Bekadja MA. The Use of CD45/SSC Dot Plots in the Classification of Acute Leukemias. J Hematol Thromb Dis. 2014;2:e107.
14. Cancer Genome Atlas Research Network. Genomic and Epigenomic Landscapes of

Adult De Novo Acute Myeloid Leukemia. N Engl J Med. 2013;368(22):2059-2074.

15. Verhaak RGW, Wouters BJ, Erpelinck CAJ, et al. Prediction of molecular subtypes in acute myeloid leukemia based on gene expression profiling. Haematologica. 2009;94(1):131-134.

16. Metzeler KH, Hummel M, Bloomfield CD, et al. An 86-probe-set gene-expression signature predicts survival in cytogenetically normal acute myeloid leukemia. Blood. 2008;112(10):4193-4201.

17. Combès E, Andrade AF, Tosi D, et al. Inhibition of Ataxia-Telangiectasia Mutated and RAD3-Related (ATR) Overcomes Oxaliplatin Resistance and Promotes Antitumor Immunity in Colorectal Cancer. Cancer Res. 2019;79(11):2933-2946.

18. Gabellier L, Bret C, Bossis G, Cartron G, Moreaux J. DNA Repair Expression Profiling to Identify High-Risk Cytogenetically Normal Acute Myeloid Leukemia and Define New Therapeutic Targets. Cancers. 2020;12(10):2874.

19. Herviou L, Kassambara A, Boireau S, et al. PRC2 targeting is a therapeutic strategy for EZ score defined high-risk multiple myeloma patients and overcome resistance to IMiDs. Clin Epigenetics. 2018;10(1):121.

20. Kassambara A, Hose D, Moreaux J, et al. Genes with a spike expression are clustered in chromosome (sub)bands and spike (sub)bands have a powerful prognostic value in patients with multiple myeloma. Haematologica. 2012;97(4):622-630.

21. Gâtel P, Brockly F, Reynes C, et al. Ubiquitin and SUMO conjugation as biomarkers of acute myeloid leukemias response to chemotherapies. Life Sci Alliance. 2020;3(6):e201900577.

22. Christopher MJ, Petti AA, Rettig MP, et al. Immune Escape of Relapsed AML Cells after Allogeneic Transplantation. N Engl J Med. 2018;379(24):2330-2341.

23. Adane B, Ye H, Khan N, et al. The Hematopoietic Oxidase NOX2 Regulates Self-Renewal of Leukemic Stem Cells. Cell Rep. 2019;27(1):238-254.

24. Schröder K. NADPH oxidases: Current aspects and tools. Redox Biol. 2020;34:101512.

25. Levy R, Rotrosen D, Nagauker O, Leto TL, Malech HL. Induction of the respiratory burst in HL-60 cells. Correlation of function and protein expression. J Immunol. 1990;145(8):2595-2601.

26. Dakik H, El Dor M, Leclerc J, et al. Characterization of NADPH Oxidase Expression and Activity in Acute Myeloid Leukemia Cell Lines: A Correlation with the Differentiation Status. Antioxidants. 2021;10(3):498.

27. Dao VT-V, Elbatreek MH, Altenhöfer S, et al. Isoform-selective NADPH oxidase inhibitor panel for pharmacological target validation. Free Radic Biol Med. 2020;148:60-69.
28. Yamamoto T, Sakaguchi N, Hachiya M, Nakayama F, Yamakawa M, Akashi M. Role of catalase in monocytic differentiation of U937 cells by TPA: hydrogen peroxide as a second messenger. Leukemia. 2009;23(4):761-769.
29. Chamulitrat W, Schmidt R, Tomakidi P, et al. Association of gp91phox homolog Nox1 with anchorage-independent growth and MAP kinase-activation of transformed human keratinocytes. Oncogene. 2003;22(38):6045-6053.
30. Thomas DC. The phagocyte respiratory burst: Historical perspectives and recent advances. Immunol Lett. 2017;192:88-96.
31. Holmström KM, Finkel T. Cellular mechanisms and physiological consequences of redox-dependent signalling. Nat Rev Mol Cell Biol. 2014;15(6):411-421.
32. Sillar JR, Germon ZP, De Iuliis GN, Dun MD. The Role of Reactive Oxygen Species in Acute Myeloid Leukaemia. Int J Mol Sci. 2019;20(23):6003.
33. Aurelius J, Thorén FB, Akhiani AA, et al. Monocytic AML cells inactivate antileukemic lymphocytes: role of NADPH oxidase/gp91phox expression and the PARP-1/PAR pathway of apoptosis. Blood. 2012;119(24):5832-5837.
34. Moloney JN, Cotter TG. ROS signalling in the biology of cancer. Semin Cell Dev Biol. 2018;80:50-64.
35. Bossis G, Sarry J-E, Kifagi C, et al. The ROS/SUMO Axis Contributes to the Response of Acute Myeloid Leukemia Cells to Chemotherapeutic Drugs. Cell Rep. 2014;7(6):1815-1823.
36. Bossis G, Melchior F. Regulation of SUMOylation by Reversible Oxidation of SUMO Conjugating Enzymes. Mol Cell. 2006;21(3):349-357.
37. Reddy MM, Fernandes MS, Salgia R, Levine RL, Griffin JD, Sattler M. NADPH oxidases regulate cell growth and migration in myeloid cells transformed by oncogenic tyrosine kinases. Leukemia. 2011;25(2):281-289.
38. Robinson AJ, Hopkins GL, Rastogi N, et al. Reactive Oxygen Species Drive Proliferation in Acute Myeloid Leukemia via the Glycolytic Regulator PFKFB3. Cancer Res. 2020;80(5):937-949.
39. Robinson AJ, Davies S, Darley RL, Tonks A. Reactive Oxygen Species Rewires Metabolic Activity in Acute Myeloid Leukemia. Front Oncol. 2021;11:632623.
40. Hole PS, Pearn L, Tonks AJ, et al. Ras-induced reactive oxygen species promote growth factor–independent proliferation in human CD34+ hematopoietic progenitor cells.

Blood. 2010;115(6):1238-1246.

41. Aydin E, Hallner A, Grauers Wiktorin H, Staffas A, Hellstrand K, Martner A. NOX2 inhibition reduces oxidative stress and prolongs survival in murine KRAS - induced myeloproliferative disease. Oncogene. 2019;38(9):1534-1543.

42. Jayavelu AK, Müller JP, Bauer R, et al. NOX4-driven ROS formation mediates PTP inactivation and cell transformation in FLT3ITD-positive AML cells. Leukemia. 2016;30(2):473-483.

43. Marlein CR, Zaitseva L, Piddock RE, et al. NADPH oxidase-2 derived superoxide drives mitochondrial transfer from bone marrow stromal cells to leukemic blasts. Blood. 2017;130(14):1649-1660.

44. Martner A, Wiktorin HG, Lenox B, et al. Histamine Promotes the Development of Monocyte-Derived Dendritic Cells and Reduces Tumor Growth by Targeting the Myeloid NADPH Oxidase. J Immunol. 2015;194(10):5014-5021.

45. Youn JY, Gao L, Cai H. The p47phox- and NADPH oxidase organiser 1 (NOXO1)-dependent activation of NADPH oxidase 1 (NOX1) mediates endothelial nitric oxide synthase (eNOS) uncoupling and endothelial dysfunction in a streptozotocin-induced murine model of diabetes. Diabetologia. 2012;55(7):2069-2079.

46. Cheng G, Ritsick D, Lambeth JD. Nox3 Regulation by NOXO1, p47phox, and p67phox*. J Biol Chem. 2004;279(33):34250-34255.

47. Brune M, Castaigne S, Catalano J, et al. Improved leukemia-free survival after postconsolidation immunotherapy with histamine dihydrochloride and interleukin-2 in acute myeloid leukemia: results of a randomized phase 3 trial. Blood. 2006;108(1):88-96.

48. Aurelius J, Martner A, Brune M, et al. Remission maintenance in acute myeloid leukemia: impact of functional histamine H2 receptors expressed by leukemic cells. Haematologica. 2012;97(12):1904-1908.

49. Altenhöfer S, Radermacher KA, Kleikers PWM, Wingler K, Schmidt HHHW. Evolution of NADPH Oxidase Inhibitors: Selectivity and Mechanisms for Target Engagement. Antioxid Redox Signal. 2015;23(5):406-427.

50. El Dor M, Dakik H, Polomski M, et al. VAS3947 Induces UPR-Mediated Apoptosis through Cysteine Thiol Alkylation in AML Cell Lines. Int J Mol Sci. 2020;21(15):5470.

51. Sun Q-A, Hess DT, Wang B, Miyagi M, Stamler JS. Off-target thiol alkylation by the NADPH oxidase inhibitor 3-benzyl-7-(2-benzoxazolyl)thio-1,2,3-triazolo[4,5-d]pyrimidine (VAS2870). Free Radic Biol Med. 2012;52(9):1897-1902.

52. Jones CL, Stevens BM, Pollyea DA, et al. Nicotinamide Metabolism Mediates

Resistance to Venetoclax in Relapsed Acute Myeloid Leukemia Stem Cells. Cell Stem Cell. 2020;27(5):748-764.

53. Gerner RR, Macheiner S, Reider S, et al. Targeting NAD immunometabolism limits severe graft-versus-host disease and has potent antileukemic activity. Leukemia. 2020;34(7):1885-1897.

54. Mitchell SR, Larkin K, Grieselhuber NR, et al. Selective targeting of NAMPT by KPT-9274 in acute myeloid leukemia. Blood Adv. 2019;3(3):242-255.

Table 1. List of the 6 probesets included in the NOX score. *Gene symbol, adjusted p-value, hazard ratio and prognosis significance are provided for each gene, as determined in the Verhaak cohort (n=504).*

Probe set	Gene symbol	MaxStat threshold	Benjamini Hochberg corrected p-value	Hazard ratio	β-coefficient	Prognosis
229445_at	CYBA	-1.121	0.0104	0.673	-0.3964	Good
203922_s_at	CYBB	-0,619	0.0511	1.263	0.2331	NS
204961_s_at	NCF1	1.108	0.0172	0.677	-0.3898	Good
209949_at	NCF2	-0,291	0.0208	1.303	0.2647	Poor
205147_x_at	NCF4	0,718	0.0169	1.359	0.3066	Poor
207419_s_at	RAC2	-0,590	0.0058	1.490	0.3987	Poor

Table 2. Cox analysis of overall survival in Verhaak training set (n=252), Verhaak test set (n=252), Metzeler validation set (n=240) and TCGA validation set (n=148) according to NOX score, cytogenetic prognosis, age and FAB classification. *Hazard ratio (HR) and p-values are shown for each parameter in univariate and multivariate Cox analysis.*

Prognostic factors		Univariate Cox analysis		Multivariate Cox analysis	
		HR	p-value	HR	p-value
Verhaak training cohort					
NOX score *(Reference : low NOX score)*	High NOX score	1.85	< 0.001	1.76	0.003
Cytogenetic & molecular prognosis *(Reference : Good)*	Intermediate	2.85	< 0.001	2.54	< 0.001
	Poor	3.97	< 0.001	3.02	< 0.001
Age *(per year)*		1.02	0.008	1.01	0.111
FAB classification *(Reference : M4 or M5)*	Not M4 or M5	0.77	0.125	0.885	0.506
Verhaak test cohort					
NOX score *(Reference : low Nox score)*	High NOX score	1.59	0.003	1.75	0.003
Cytogenetic & molecular prognosis *(Reference : Good)*	Intermediate	1.32	0.242	1.20	0.450
	Poor	2.78	< 0.001	2.53	0.001
Age *(per year)*		1.01	0.095	1.01	0.381
FAB classification *(Reference : M4 or M5)*	Not M4 or M5	1.09	0.639	1.38	0.088
Metzeler validation cohort					
NOX score *(Reference : low Nox score)*	High NOX score	1.53	0.009	1.41	0.04
Cytogenetic & molecular prognosis *(Reference : Good)*	Intermediate	2.62	< 0.001	2.77	< 0.001
	Poor	3.31	< 0.001	3.61	< 0.001
Age *(per year)*		1.02	< 0.001	1.03	< 0.001
FAB classification *(Reference : M4 or M5)*	Not M4 or M5	1.30	0.145	0.91	0.632
TCGA validation cohort					
NOX score *(Reference : low Nox score)*	High NOX score	1.81	0.007	1.57	0.047
Cytogenetic & molecular prognosis *(Reference : Good)*	Intermediate	3.50	< 0.001	2.98	0.003
	Poor	5.04	< 0.001	4.14	< 0.001
Age *(per year)*		1.02	0.004	1.02	0.040
FAB classification *(Reference : M4 or M5)*	Not M4 or M5	0.93	0.765	1.02	0.923

Figure 1: Transcriptional reprogramming upon acquisition of chemoresistance by HL-60 AML cells. RNA-Seq were performed on mRNAs purified in 3 independent experiments conducted with HL-60 cells and their Ara-C-resistant (ARA-R) and DNR-resistant (DNR-R) population derivatives. (A) Venn diagram for up-regulated (>2 fold, FDR<0.05) and down-regulated (>2 fold, FDR<0.05) genes in ARA-R and DNR-R cells compared to parental HL-60 cells. (B) Volcano plot for Differentially Expressed Genes (DEGs) between DNR-R- and HL-60 cells. Blue dots correspond to the DEGs in DNR-R but not in ARA-R cells, red dots to DEGs in DNR-R cells that are up-regulated in ARA-R cells and green dots to DEGs that are down-regulated in ARA-R cells. (C) Volcano plot for DEGs between ARA-R- and HL-60 cells. Blue dots correspond to the DEGs in ARA-R but not in DNR-R cells, yellow dots to DEGs in ARA-R cells that are up-regulated in DNR-R cells and purple dots to DEGs in ARA-R cells that are down-regulated in DNR-R cells. (D) Gene Ontology analysis of genes up-regulated in both DNR-R and ARA-R cells compared to parental HL-60 cells. (E) Gene Set Enrichment Analysis (GSEA) was performed using RNA-Seq data from ARA-R, DNR-R- and parental HL-60 cells. The enrichment for the "inflammatory response" signature (175 genes) is shown. NES (normalized enrichment score), nominal p-value and FDR (false decision rate) are presented. (F) The inflammatory signature (175 genes) identified in (E) was used in GSEA analysis with RNA-Seq data from 3 patients from the FAB M2 subtype obtained from a publicly available cohort [22].

Figure 2: NOX2 expression and activity are increased in DNR-resistant HL-60 cells. (A) The NAPDH oxidase NOX2 is composed of two membrane-associated proteins, $gp91^{phox}$ and $p22^{phox}$. Upon activation, the cytosolic subunits $p67^{phox}$, $p47^{phox}$ and $p40^{phox}$ translocate to the membrane together with the small GTPase Rac2 to form the full oxidase complex. (B) Heatmap of the RNA-seq data in parental, DNR-R and ARA-R cells showing the expression of the genes encoding the NOX2 subunits (*CYBB*, *CYBA*, NCF1, *NCF2*, *NCF4*, *RAC2*). (C) The expression of *CYBB* and *NCF2* was analyzed by RT-qPCR on mRNA purified from parental-, ARA-R- and DNR-R cells and normalized to *S26* mRNA levels. Data are presented as percentages of the HL-60 condition (n=5, mean +/- SD). (D,E) Parental, ARA-R and DNR-R HL-60 (D) or U937 (E) cells were treated or not with PMA and the production of ROS was measured by following L-012 luminescence over 2 hours (n=4 for HL-60, n=3 for U937, a representative experiment is shown). (F) The expression of *CYBB* and *NCF2* was analyzed by RT-qPCR on mRNA purified from parental-, ARA-R- and DNR-R cells and normalized to *S26* mRNA levels. Data are presented as percentages of the U937 condition

(n=4, mean +/- SD). gp91^{phox} surface expression was measured by flow cytometry in parental, DNR-R and ARA-R U937 cells. The median fluorescence intensity (MFI) obtained with isotypic controls was subtracted to the gp91 MFI and normalized to the parental cells (n=6, mean +/- SD).

Figure 3: Overexpression of NADPH oxidase components is responsible for increased ROS production in chemoresistant AML cells. (A-C) DNR-R and ARA-R HL-60 cell populations were cloned and 14 clones for each were used to measure mRNA expression for *CYBB* (A) and *NCF2* (B) using RT-qPCR. Data were normalized to *S26* mRNA levels and are presented as ratios to parental HL-60 cells (n=3, mean +/- SD). (C) ROS production was measured after addition of PMA using L-012 luminescence. The AUC (Area Under Curve) was calculated after plotting L-012 luminescence over 1 hr (n=3, mean +/- SD). (D) gp91^{phox} surface expression was measured by flow cytometry in parental HL-60 cells as well as in two DNR-R clones showing high NADPH oxidase activity (15165 and 15176) and two clones with low NADPH oxidase activity (15160 and 15169). (E) DNR-R clones 15165 and 15176 were stimulated or not with PMA with or without VAS2870 and ROS production was measured by luminometry (n=3, a representative experiment is shown).

Figure 4: NOX2 overexpression participates in the acquisition/maintenance of resistance to DNR. (A) gp91^{phox} surface expression was measured by flow cytometry in parental HL-60 cells, in DNR-R clones (15165) as well as 15165 cells CRISPR/Cas9 KO for gp91^{Phox} and 15165 cells subjected to mock CRISPR/Cas9 mutagenesis. (B) NADPH oxidase activity was detected by ROS measurement in the cells presented in (A) after PMA addition using L-012 luminescence. (n=3, a representative experiment is shown). (C) Cell proliferation was measured using MTS (n=3, mean +/- SD). (D) IC_{50} for DNR was measured after 24 hrs of treatment using MTS (n=4, mean +/- SD). (E, F) HL60 and two DNR-R clones (15165 and 15176) were cultured in the presence of SOD (30 U/mL) and Catalase (25 µg/mL) for 3 weeks. (E) The number of cells was then measured using MTS and represented as a ratio to the mock treated cells (n=5, mean +/- SD). (F) IC_{50} for DNR was measured after 24 hrs of DNR treatment using MTS (n=4, mean +/- SD). All p-values were calculated with One-way Anova and Tukey's multiple comparison test.

Figure 5: NOX2 expression and activity is higher in FAB M4/M5 patients. (A) gp91^{phox} expression (MFI) was measured by flow cytometry on the leukemic cells (CD45/SSC gating)

present in bone marrow aspirates taken at diagnosis from 74 AML patients. Patients are classified according to the FAB classification. The median is represented as a horizontal line for each group. p=0.0057 in one-way Anova (Kruskal-Wallis test) (B) mRNA expression for *CYBB* gene was measured by RNA-Seq in the TCGA cohort comprising 198 AML patients. (C) $gp91^{phox}$ surface expression was measured by flow cytometry on AML cells from two patients sorted using CD45/SSC gating and separated according to their level of expression of the CD34 marker. (D) Sorted AML cells ($CD34^+$ and $CD34^-$) for each patient were used to measure ROS production after stimulation with PMA (10 nM). (E) $gp91^{phox}$ expression (MFI) was measured by flow cytometry on leukemic cells (CD45/SSC gating) present in bone marrow aspirates taken at diagnosis and after the induction chemotherapy (between 15 and 45 days after the beginning of the treatment) from 8 AML patients (Supplementary Table 3, ID numbers of the patients indicated on the figure). Four of the patients reached CR after induction chemotherapy (16119, 16127, 16185, 17235), two reached CR after allograft (14056 and 16126) and two never reached CR (17202, 17217). All patients but one (17235, who was allografted) relapsed.

Figure 6: Identification of a NOX score with prognosis value in AML. (A) Patients of the Verhaak training cohort comprising 252 patients were ranked according to increasing NOX score. The cut-point of 0.41 was selected using the MaxStat R function to obtain a maximum difference in overall survival (OS) between the two groups. Kaplan-Meyer survival curves were established using the cut-point value of 0.41 in the training cohort. (B-D) The NOX-score was validated in three independent cohorts using the 0.41 cutpoint. (E) Gene Set Enrichment Analysis (GSEA) was performed using RNA-Seq data from chemoresistant (ARA-R and DNR-R) compared to parental HL-60 cells. The gene list comprises the 50 most up-regulated genes in the 10% of patients with the highest NOX score, compared to the 50% patients with the lowest NOX score in the Verhaak cohort. NES (normalized enrichment score) and nominal p-value are presented. (F) Expression of *CYBB*, *NCF1*, *NCF2* and *NAMPT* in 200 patient samples from the TCGA cohort. R represents the Pearson rho correlation coefficient between the expression of *NCF1*, *NCF2* or *NAMPT* and *CYBB.*

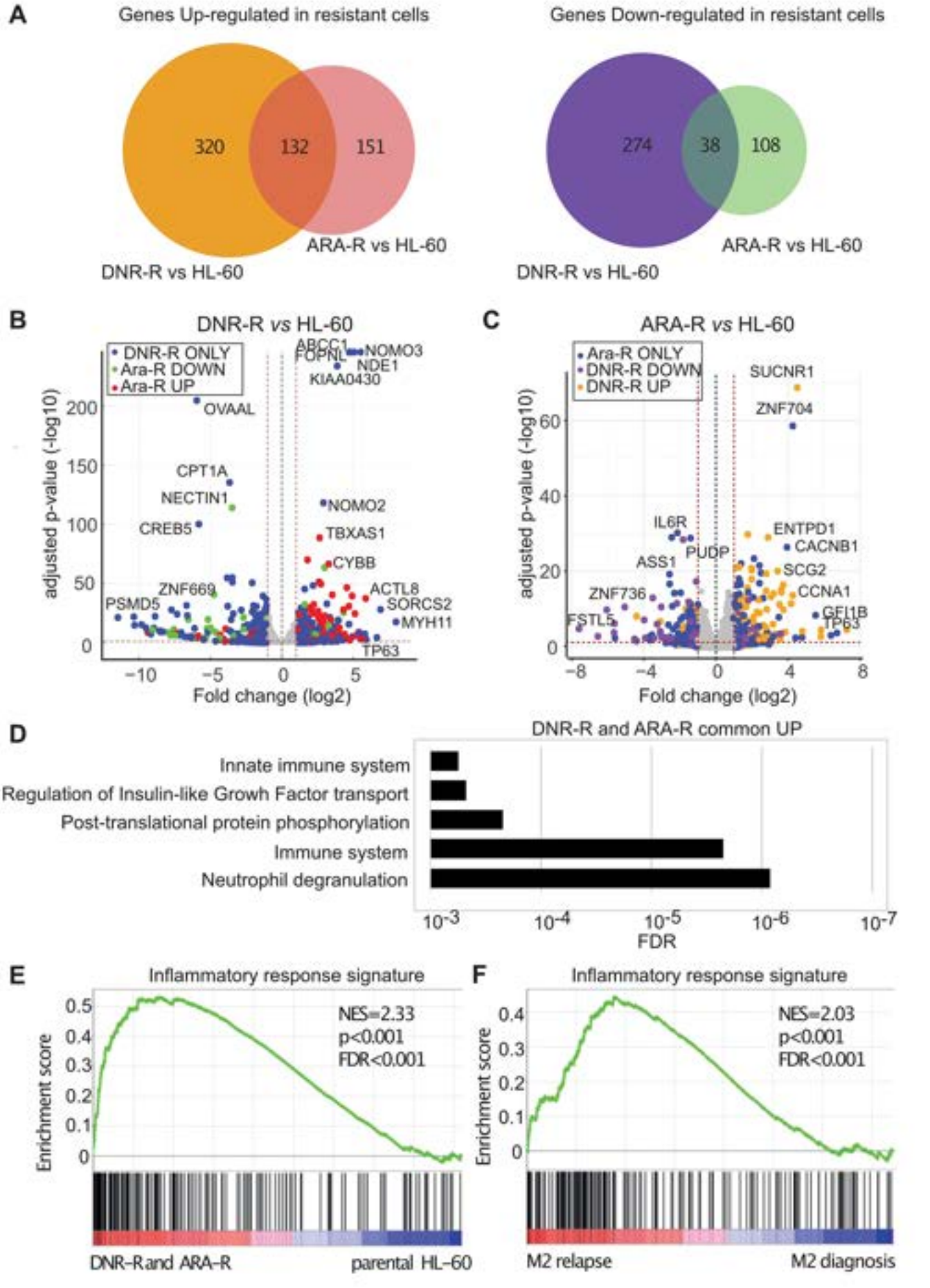
A
Genes Up-regulated in resistant cells
320
132
151
DNR-R vs HL-60
ARA-R vs HL-60
Genes Down-regulated in resistant cells
274
38
108
DNR-R vs HL-60
ARA-R vs HL-60
B
DNR-R vs HL-60
DNR-R ONLY
Ara-R DOWN
Ara-R UP
adjusted p-value (-log10)
Fold change (log2)
OVAAL
CPT1A
NECTIN1
CREB5
ZNF669
PSMD5
ABCC1
FOPNL
NOMO3
NDE1
KIAA0430
NOMO2
TBXAS1
CYBB
ACTL8
SORCS2
MYH11
TP63
C
ARA-R vs HL-60
Ara-R ONLY
DNR-R DOWN
DNR-R UP
adjusted p-value (-log10)
Fold change (log2)
SUCNR1
ZNF704
IL6R
PUDP
ASS1
ZNF736
FSTL5
ENTPD1
CACNB1
SCG2
CCNA1
GFI1B
TP63
D
DNR-R and ARA-R common UP
Innate immune system
Regulation of Insulin-like Growh Factor transport
Post-translational protein phosphorylation
Immune system
Neutrophil degranulation
FDR
E
Inflammatory response signature
Enrichment score
NES=2.33
p<0.001
FDR<0.001
DNR-Rand ARA-R
parental HL-60
F
Inflammatory response signature
Enrichment score
NES=2.03
p<0.001
FDR<0.001
M2 relapse
M2 diagnosis

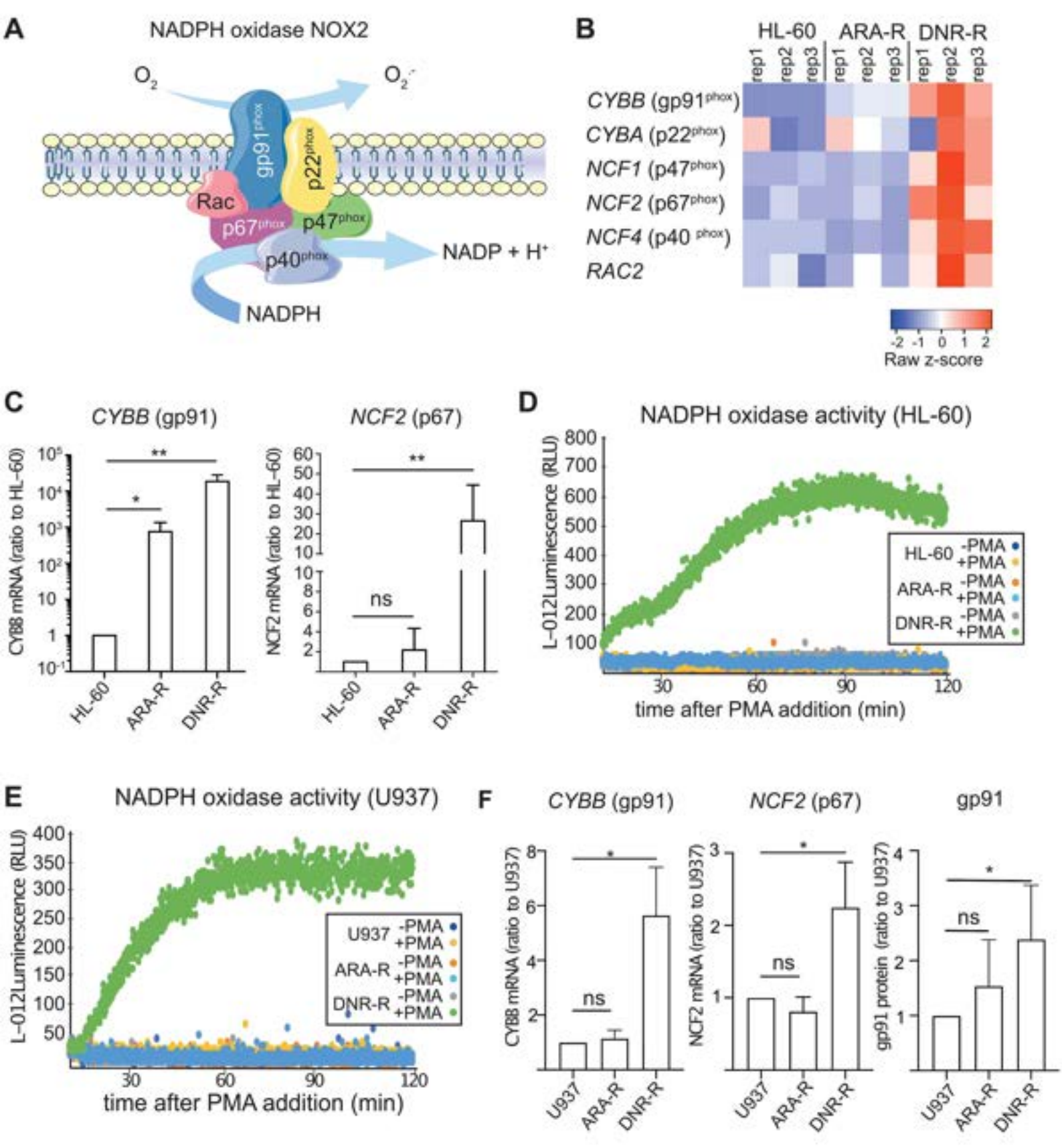
A
NADPH oxidase NOX2
O2
O2-
gp91phox
p22phox
Rac
p67phox
p47phox
p40phox
NADP + H+
NADPH
B
HL-60
ARA-R
DNR-R
rep1
rep2
rep3
CYBB (gp91phox)
CYBA (p22phox)
NCF1 (p47phox)
NCF2 (p67phox)
NCF4 (p40 phox)
RAC2
-2 -1 0 1 2
Raw z-score
C
CYBB (gp91)
NCF2 (p67)
CYBB mRNA (ratio to HL-60)
NCF2 mRNA (ratio to HL-60)
ns
HL-60
ARA-R
DNR-R
D
NADPH oxidase activity (HL-60)
L-012Luminescence (RLU)
time after PMA addition (min)
HL-60 -PMA +PMA
ARA-R -PMA +PMA
DNR-R -PMA +PMA
E
NADPH oxidase activity (U937)
L-012Luminescence (RLU)
time after PMA addition (min)
U937 -PMA +PMA
ARA-R -PMA +PMA
DNR-R -PMA +PMA
F
CYBB (gp91)
NCF2 (p67)
gp91
CYBB mRNA (ratio to U937)
NCF2 mRNA (ratio to U937)
gp91 protein (ratio to U937)
ns
U937
ARA-R
DNR-R

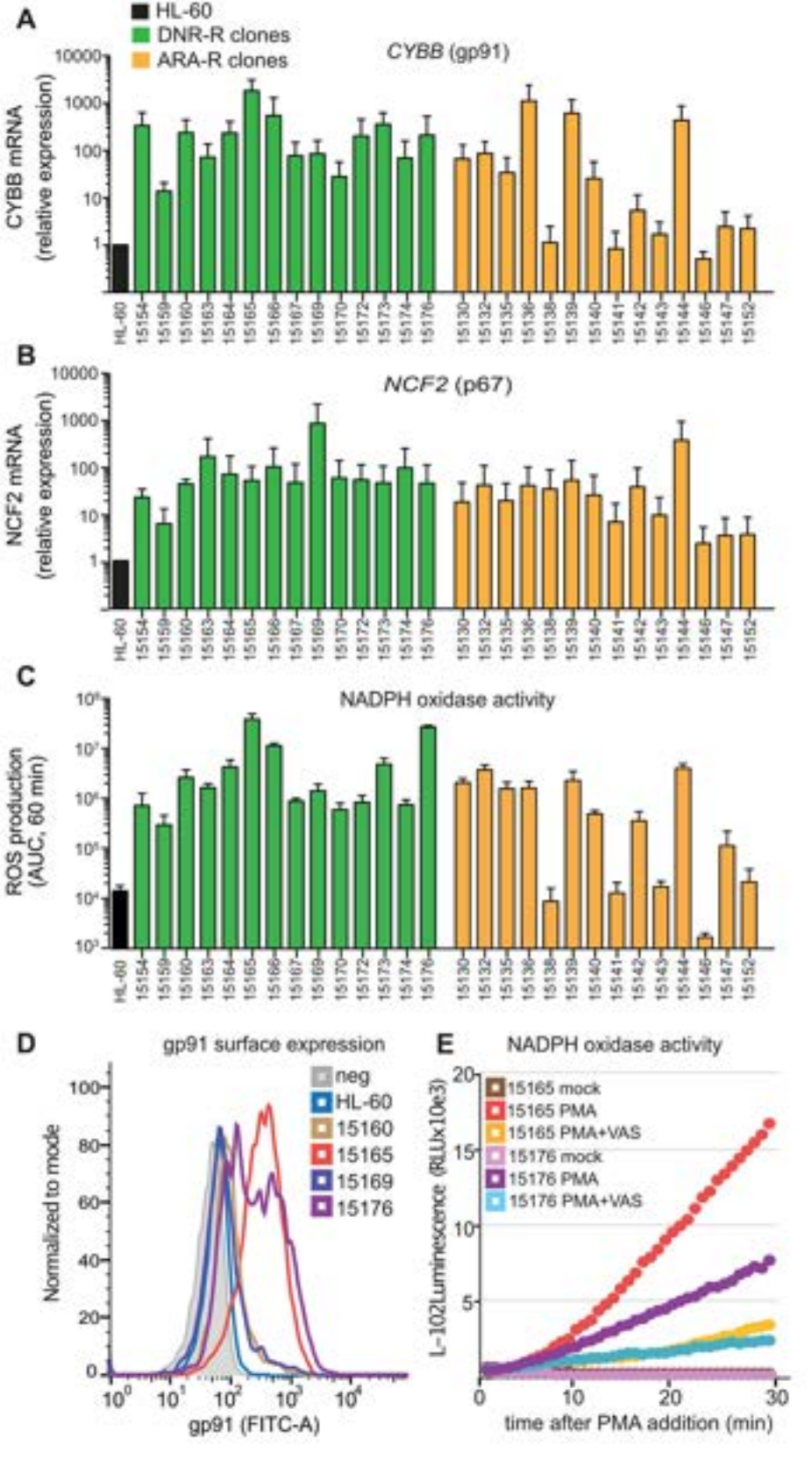
A
HL-60
DNR-R clones
ARA-R clones
CYBB (gp91)
CYBB mRNA (relative expression)
10000
1000
100
10
1
HL-60
15154
15159
15160
15163
15164
15165
15166
15167
15169
15170
15172
15173
15174
15176
15130
15132
15135
15136
15138
15139
15140
15141
15142
15143
15144
15146
15147
15152
B
NCF2 (p67)
NCF2 mRNA (relative expression)
C
NADPH oxidase activity
ROS production (AUC, 60 min)
D
gp91 surface expression
neg
HL-60
15160
15165
15169
15176
Normalized to mode
gp91 (FITC-A)
E
NADPH oxidase activity
15165 mock
15165 PMA
15165 PMA+VAS
15176 mock
15176 PMA
15176 PMA+VAS
L-102Luminescence (RLUx10e3)
time after PMA addition (min)

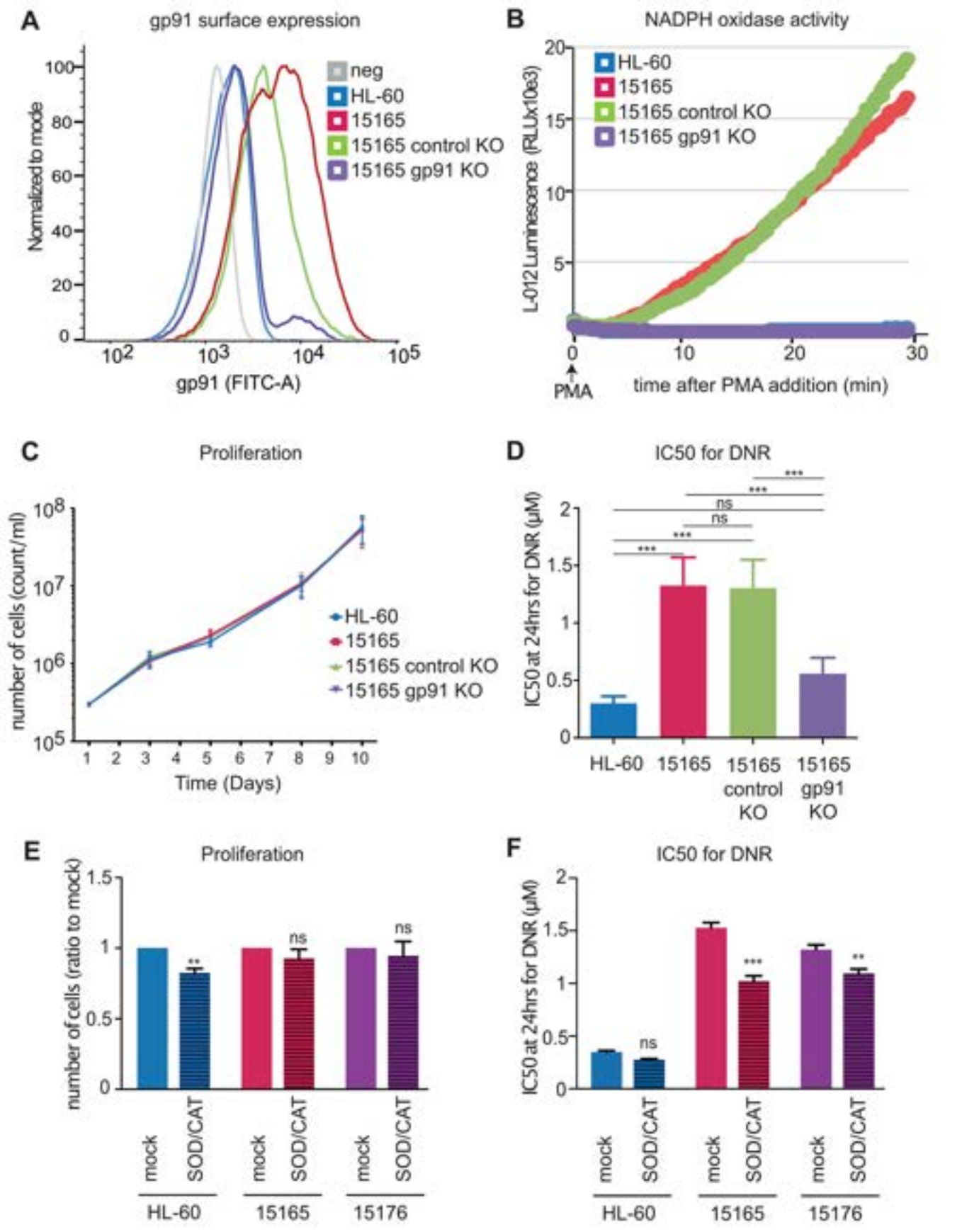
A
gp91 surface expression
Normalized to mode
gp91 (FITC-A)
neg
HL-60
15165
15165 control KO
15165 gp91 KO
B
NADPH oxidase activity
L-012 Luminescence (RLUx10e3)
time after PMA addition (min)
PMA
C
Proliferation
number of cells (count/ml)
Time (Days)
D
IC50 for DNR
IC50 at 24hrs for DNR (μM)
ns
E
Proliferation
number of cells (ratio to mock)
mock
SOD/CAT
HL-60
15165
15176
F
IC50 for DNR
IC50 at 24hrs for DNR (μM)

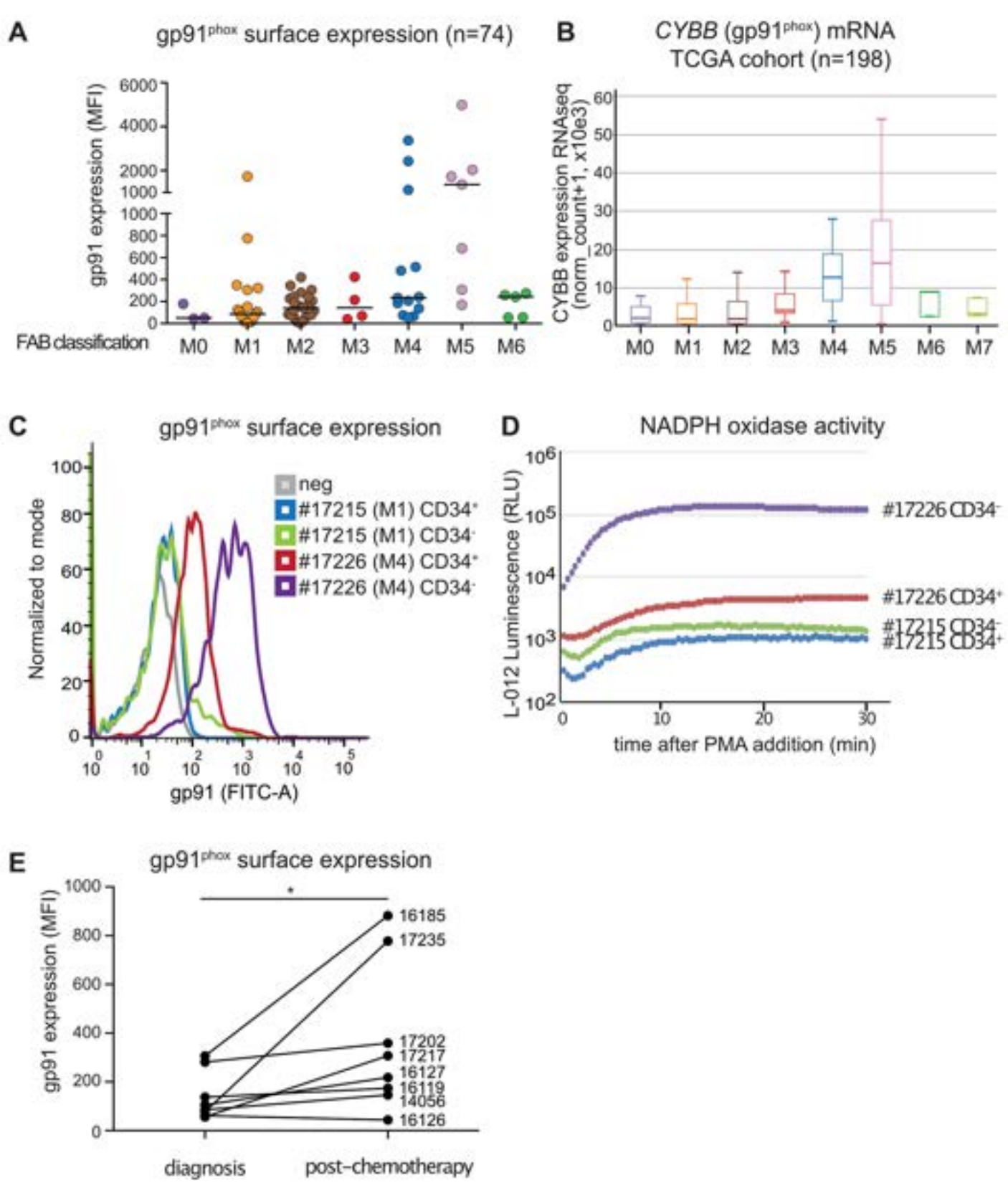
A
gp91phox surface expression (n=74)
gp91 expression (MFI)
FAB classification
M0
M1
M2
M3
M4
M5
M6
B
CYBB (gp91phox) mRNA
TCGA cohort (n=198)
CYBB expression RNAseq
(norm_count+1, x10e3)
M7
C
gp91phox surface expression
Normalized to mode
neg
#17215 (M1) CD34+
#17215 (M1) CD34-
#17226 (M4) CD34+
#17226 (M4) CD34-
gp91 (FITC-A)
D
NADPH oxidase activity
L-012 Luminescence (RLU)
#17226 CD34-
#17226 CD34+
#17215 CD34-
#17215 CD34+
time after PMA addition (min)
E
gp91phox surface expression
gp91 expression (MFI)
16185
17235
17202
17217
16127
16119
14056
16126
diagnosis
post-chemotherapy

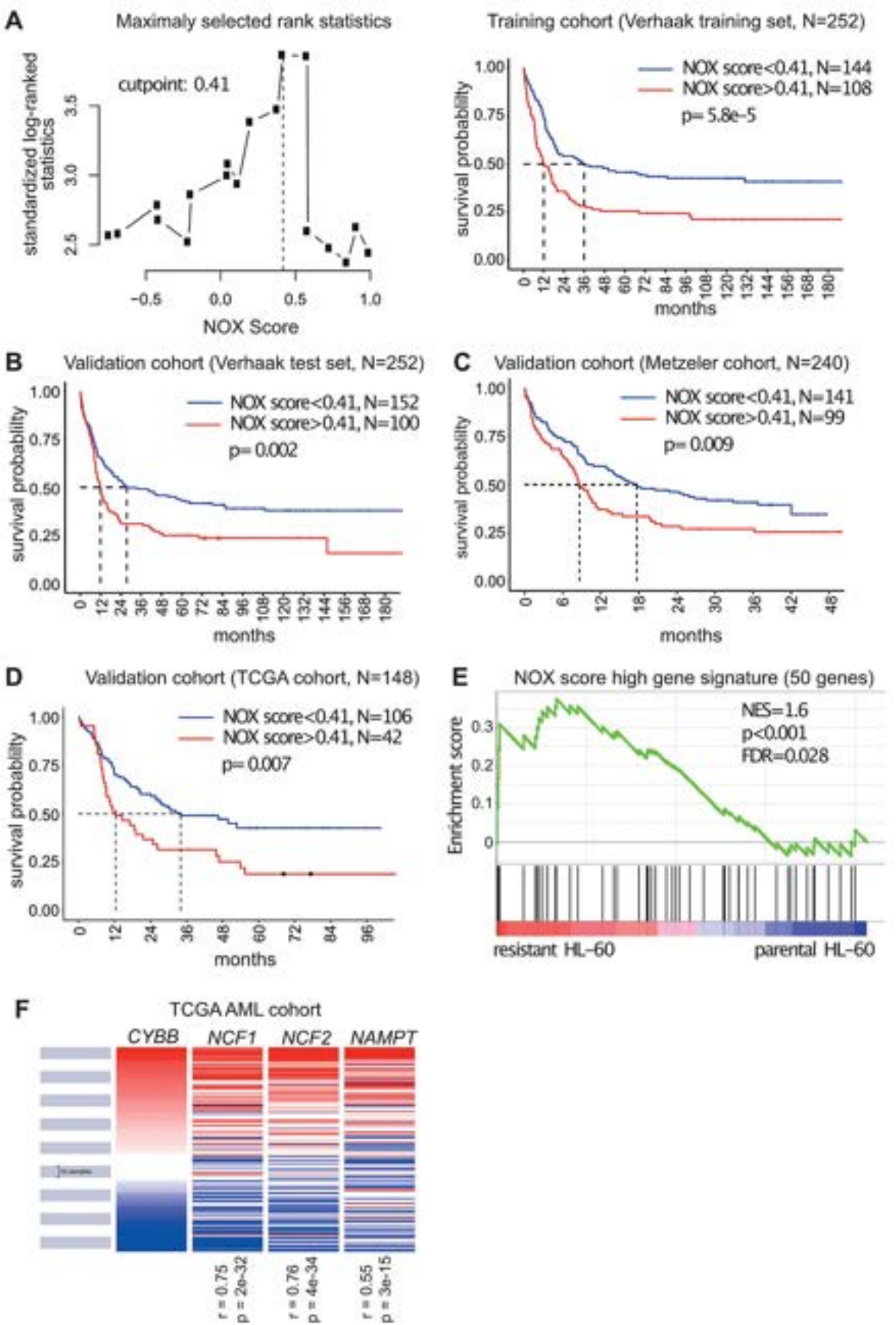
A
Maximaly selected rank statistics
cutpoint: 0.41
standardized log-ranked statistics
NOX Score
Training cohort (Verhaak training set, N=252)
NOX score<0.41, N=144
NOX score>0.41, N=108
p= 5.8e-5
survival probability
months
B
Validation cohort (Verhaak test set, N=252)
NOX score<0.41, N=152
NOX score>0.41, N=100
p= 0.002
C
Validation cohort (Metzeler cohort, N=240)
NOX score<0.41, N=141
NOX score>0.41, N=99
p= 0.009
D
Validation cohort (TCGA cohort, N=148)
NOX score<0.41, N=106
NOX score>0.41, N=42
p= 0.007
E
NOX score high gene signature (50 genes)
NES=1.6
p<0.001
FDR=0.028
Enrichment score
resistant HL-60
parental HL-60
F
TCGA AML cohort
CYBB
NCF1
NCF2
NAMPT
r = 0.75
p = 2e-32
r = 0.76
p = 4e-34
r = 0.55
p = 3e-15

Supplementary Methods

Pharmacological inhibitors and reagents

Cytosine-β-D-arabinofuranoside (Ara-C), daunorubicin-hydrochloride (DNR) and Phorbol 12-myristate-13-acetate (PMA) were purchased from Sigma-Aldrich. The NADPH oxidase inhibitor VAS2870 was from Enzo Life Sciences. L-012 was from Sobioda (ref W1W120-04891).

Cell culture

HL-60 cell line originates from a patient with AML with maturation (FAB-M2)[1]. U937 is a monocytic cell line originating from a patient with diffuse histiocytic lymphoma[2]. HL-60 and U937 cells were cultured at 37°C in RPMI medium supplemented with 10 % fetal bovine serum (FBS) and streptomycin/penicillin in the presence of 5 % CO_2. Both cell lines were authenticated by the ATCC using Short-Tandem-Repeat analysis. HL-60 and U937 cells resistant to Ara-C and DNR were generated by culturing them in the presence of increasing concentrations of drugs (from 1 nM up to 100 nM for Ara-C and 30 nM for DNR) for 2-3 months[3]. Parental HL-60 cells and resistant HL-60 populations were then cloned using an Aria IIU cell sorter (Becton Dickinson). After amplification, clones were cultured for a maximum of 10 passages.

Cell proliferation and IC_{50} measurement

Cells were seeded at a concentration of $3x10^5$/mL in RPMI medium on day 0 and the number of cells was measured every two-three days using MTS assay (Promega). For IC_{50} measurements, medium was complemented with increasing doses of DNR (Sigma-Aldrich). Viability was measured 24 hours later using MTS assay. IC_{50} were calculated using the GraphPad PRISM software.

NOX activity measurement

$5x10^5$ cells were washed in PBS, resuspended in 100 µL of PBS containing 10 mM glucose and 1mM $CaCl_2$ prewarmed at 37°C and transferred to a white 96-well plate. PMA (100 nM) and VAS2870 (10 µM) were then added to the wells. The luminescent ROS indicator L-012 was then added at a final concentration of 500 µM and luminescence was recorded on a Centro XS^3 LB 960 luminometer (Berthold Technologies).

RT-qPCR assays

Total mRNA was purified using the GenElute Mammalian Total RNA kit (Sigma-Aldrich). After DNase I treatment, 1 µg of total RNA was used for cDNA synthesis using the Maxima First Strand cDNA kit (ThermoFisher Scientific). qPCR assays were conducted using Taq platinum (Invitrogen) and the LightCycler 480 device (Roche) with specific DNA primers (IDT, sequence available on request). Data were normalized to the housekeeping *S26* or *GAPDH* mRNA levels.

RNA-seq mapping, quantification and differential analysis

RNA-seq reads were mapped on the Human reference genome (hg19, GRCh37p13) using TopHat2 (2.1.1)[4] based on the Bowtie2 (2.3.5.1) aligner[5]. The reproducibility of replicates was verified using cufflinks v2.2.1 tool[6] with the linear regression of reads per kilobase per million mapped reads (RPKM) between 2 replicates. Reads association with annotated gene regions was done with the HTseq-count tool v0.11.1[7]. Differential expression analysis was performed with DESeq2[8] using normalization by sequencing depth and parametric negative binomial law to estimate the data dispersion. Genes with a fold change ≥ 2 and an adjusted p-value (FDR) < 0.05 were considered as differentially expressed genes (DEGs).

GSEA, Gene Ontology and co-expression analysis

Ontology analyses were performed using the Panther software[9] (http://www.pantherdb.org/). Gene Set Enrichment Analyses were performed using https://www.gsea-msigdb.org/gsea/index.jsp (version 4.0.3)[10]. Coexpression analyses were performed using the UCSC Xena browser (https://xenabrowser.net/heatmap/) with publicly available data from the Cancer Genome Atlas Program (TCGA)[11].

CRISPR/Cas9 knock-out of CYBB

A control or a *CYBB*-binding Cr-RNA (sequence available on request) was transfected together with a recombinant GFP-Cas9 protein and TracrRNA ATTO 550 (IDT) in HL-60 cells using the Amaxa technology. Twelve hours after transfection, GFP-positive cells were sorted and cloned. The DNA sequence surrounding the targeted CYBB sequence was PCR-amplified on genomic DNA from the selected clones, cloned in the TOPO-TA vector (Life Technologies) and sequenced.

Statistical analyses

Results are presented as means ± S.D of at least 3 biologically-independent experiments. Statistical analyses were performed using the Student t-test or One Way Anova with the

GraphPad Prism software and R.3.6.0 software (R foundation for Statistical Computing, Vienna, Austria). *; **; *** correspond to $P < 0.05$; $P < 0.01$; $P < 0.001$, respectively. ns=not significant. Statistical analyses for the RNA-Seq experiments, GSEA and NOX score are described in the relevant sections.

Supplementary References

1. Dalton Jr WT, Ahearn MJ, McCredie KB, Freireich EJ, Stass SA, Trujillo JM. HL-60 Cell Line Was Derived From a Patient With FAB-M2 and Not FAB-M3. Blood 1988;71(1):242–247.
2. Sundström C, Nilsson K. Establishment and characterization of a human histiocytic lymphoma cell line (U-937). International Journal of Cancer 1976;17(5):565–577.
3. Gâtel P, Brockly F, Reynes C, et al. Ubiquitin and SUMO conjugation as biomarkers of acute myeloid leukemias response to chemotherapies. Life Sci Alliance;3(6):.
4. Kim D, Pertea G, Trapnell C, Pimentel H, Kelley R, Salzberg SL. TopHat2: accurate alignment of transcriptomes in the presence of insertions, deletions and gene fusions. Genome Biol 2013;14(4):R36.
5. Langmead B, Salzberg SL. Fast gapped-read alignment with Bowtie 2. Nat Methods 2012;9(4):357–359.
6. Trapnell C, Roberts A, Goff L, et al. Differential gene and transcript expression analysis of RNA-seq experiments with TopHat and Cufflinks. Nat Protoc 2012;7(3):562–578.
7. Anders S, Pyl PT, Huber W. HTSeq—a Python framework to work with high-throughput sequencing data. Bioinformatics 2015;31(2):166–169.
8. Love MI, Huber W, Anders S. Moderated estimation of fold change and dispersion for RNA-seq data with DESeq2. Genome Biol;15(12):.
9. Mi H, Muruganujan A, Ebert D, Huang X, Thomas PD. PANTHER version 14: more genomes, a new PANTHER GO-slim and improvements in enrichment analysis tools. Nucleic Acids Res 2019;47(D1):D419–D426.
10. Subramanian A, Tamayo P, Mootha VK, et al. Gene set enrichment analysis: A knowledge-based approach for interpreting genome-wide expression profiles. PNAS 2005;102(43):15545–15550.
11. Cancer Genome Atlas Research Network. Genomic and Epigenomic Landscapes of Adult De Novo Acute Myeloid Leukemia. New England Journal of Medicine 2013;368(22):2059–2074.
12. Christopher MJ, Petti AA, Rettig MP, et al. Immune Escape of Relapsed AML Cells after Allogeneic Transplantation. New England Journal of Medicine 2018;379(24):2330–2341.

Supplementary Figures

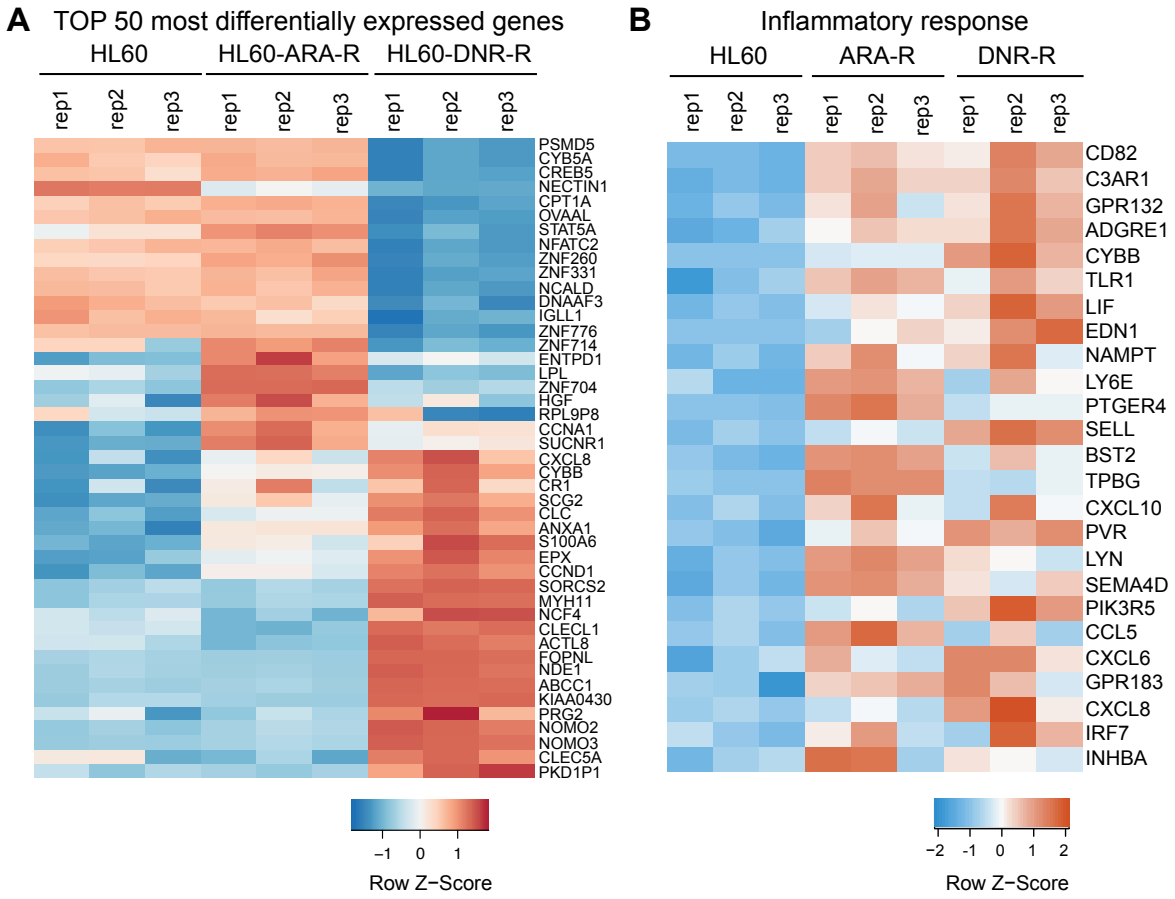

Figure S1: Genes activated in chemoresistant AML cell lines are linked with the inflammatory response. (A) Heatmap for the 50 most differentially expressed genes between parental-, DNR-R- and ARA-R cells. All biological replicates are shown. (B) Heatmap for the top 25 genes from the "inflammatory response" signature in ARA-R, DNR-R and parental HL-60 cells.

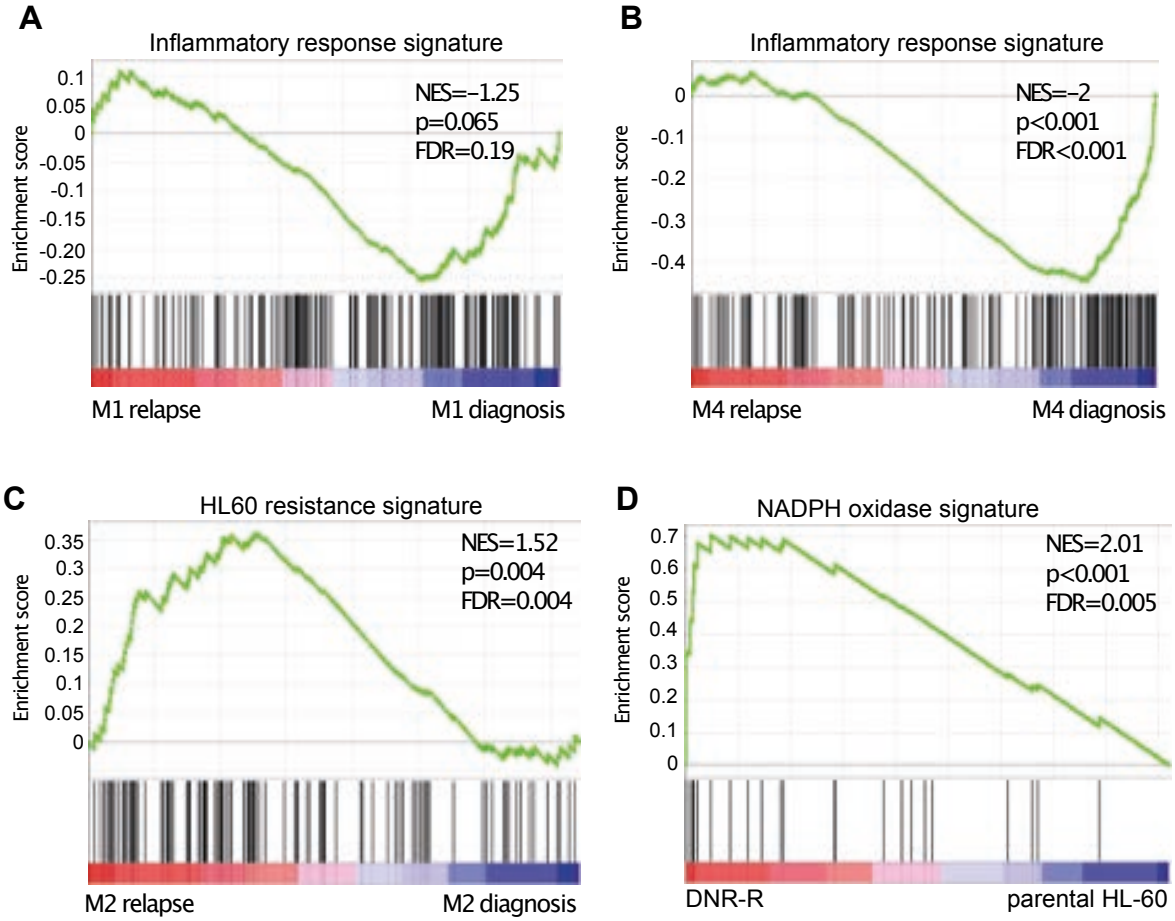

Figure S2. The inflammatory signature is not enriched in FAB M1 and M4 subtypes and a chemoresistance signature is enriched in FAB M2 patients at relapse (A,B) The inflammatory signature (175 genes) was used in GSEA analysis with RNA-Seq data from 3 patients from the FAB M1 (A) or FAB M4 (B) subtype obtained from a publicly available cohort (C) The list of genes induced in both DNR-R and ARA-R compared to parental HL-60 was used in GSEA analysis with RNA-Seq data from 3 patients from the FAB M2 subtype obtained from a publicly available cohort [12]. (D) GSEA was performed using RNA-Seq data from DNR-R and parental HL-60 cells. The enrichment for the "NADPH oxidase" signature (23 genes) is shown. NES (normalized enrichment score), nominal p-value and FDR are presented.

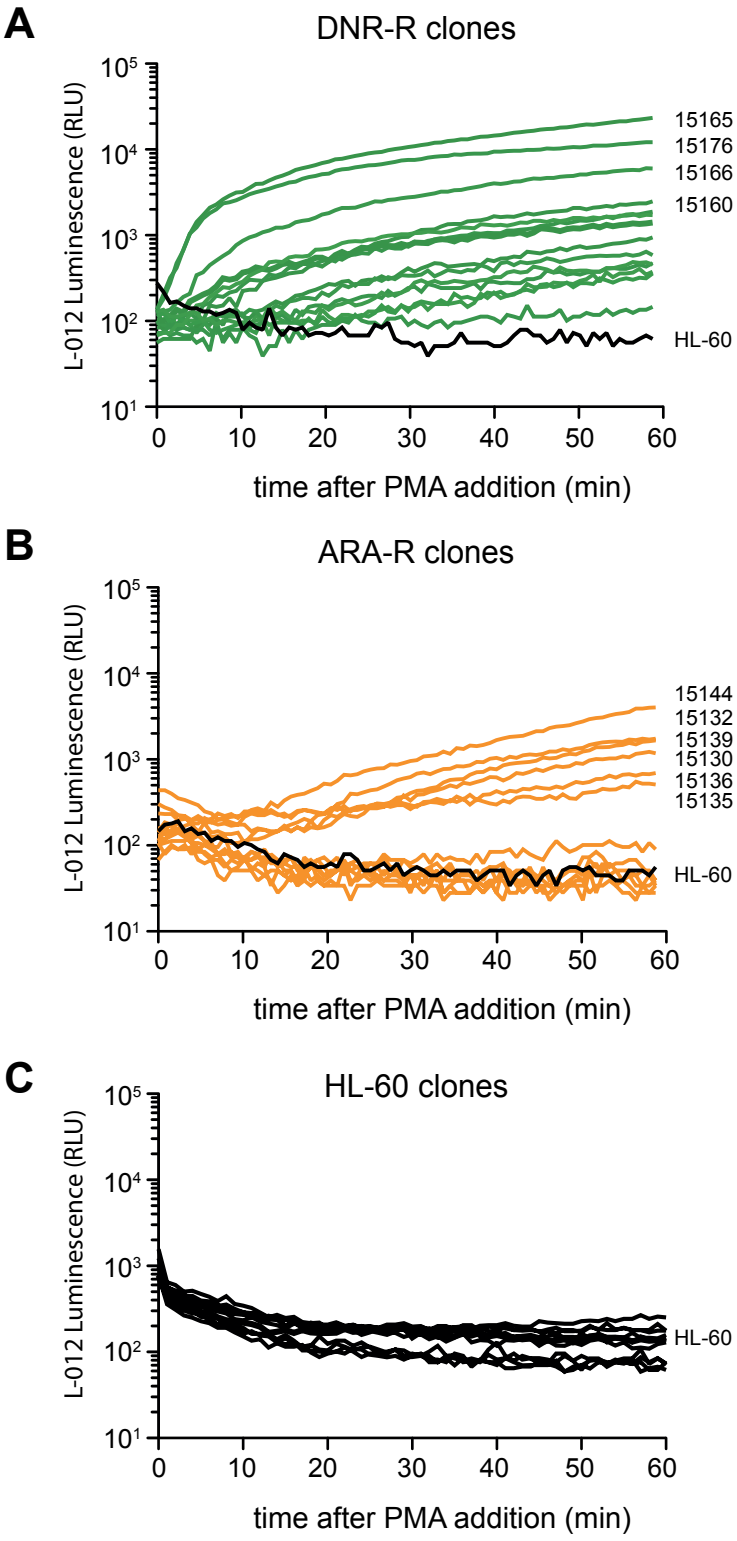

Figure S3: Measurement of NOX2 activity in parental and chemoresistant HL60 clones. ROS production was measured after addition of PMA using L-012 luminescence in (A) DNR-R, (B) ARA-R and (C) HL-60 clones over 1 hr (n=3, a representative experiment is shown).

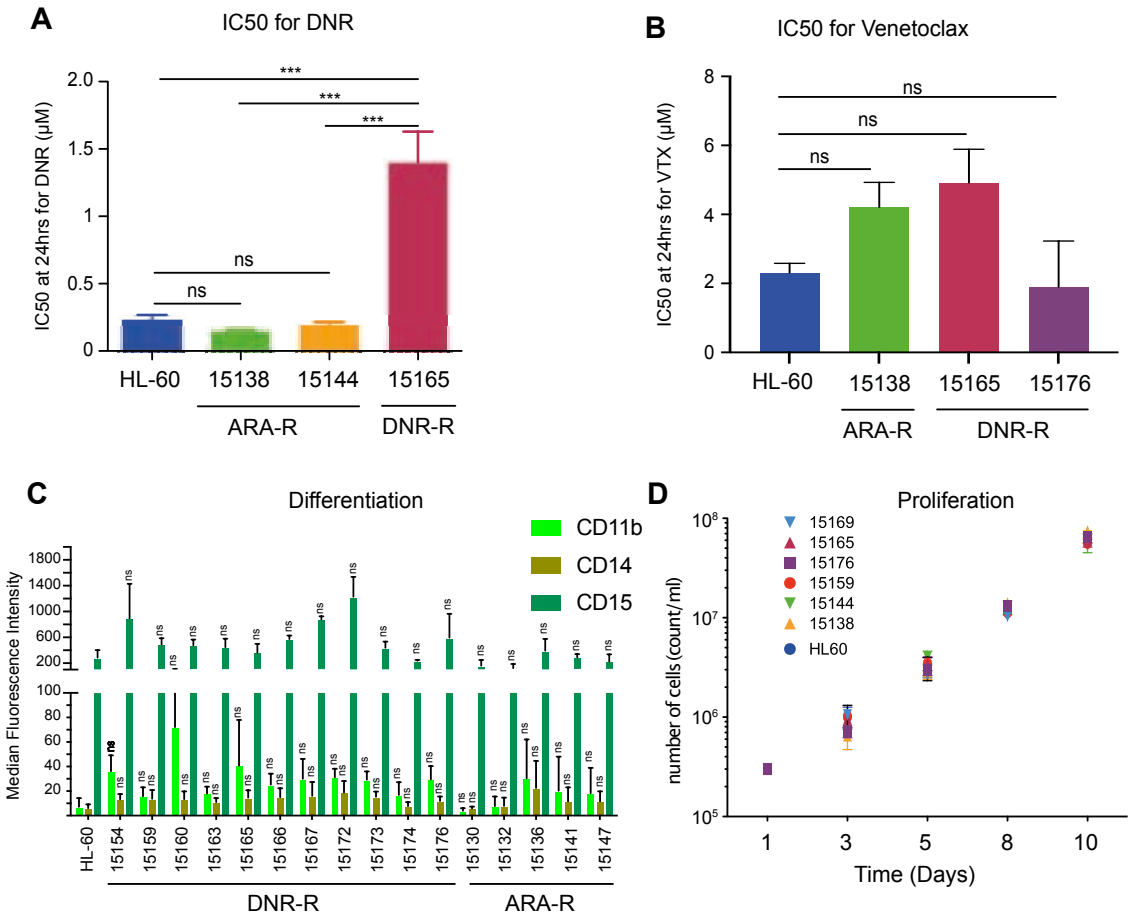

Figure S4: Cross-resistance, proliferation and differentiation of chemoresistant HL-60 clones. (A, B) IC_{50} for DNR (A) or Venetoclax (B) was measured for the indicated cells after 24 hrs of DNR treatment using MTS (n=4 for DNR, n=3 for Venetoclax, mean +/- SD). (C) Parental HL60, DNR-R and ARA-R clones were analyzed by flow cytometry for the expression of CD11b, CD14 and CD15 using CD11b-APC, CD14-PE and CD15-PECy7 antibodies (Miltenyi Biotech). Median Fluorescence Intensities are expressed as ratio to unstained cells (n=3 for CD11b and CD14, n=2 for CD15, mean +/- SD). P-values were calculated using One-way Anova with Dunnett's multiple comparison testing. (D) Cells were seeded at $3x10^5$ on the first day and their proliferation was followed using MTS every 2-3 days for 10 days (n=3, mean +/-SD).

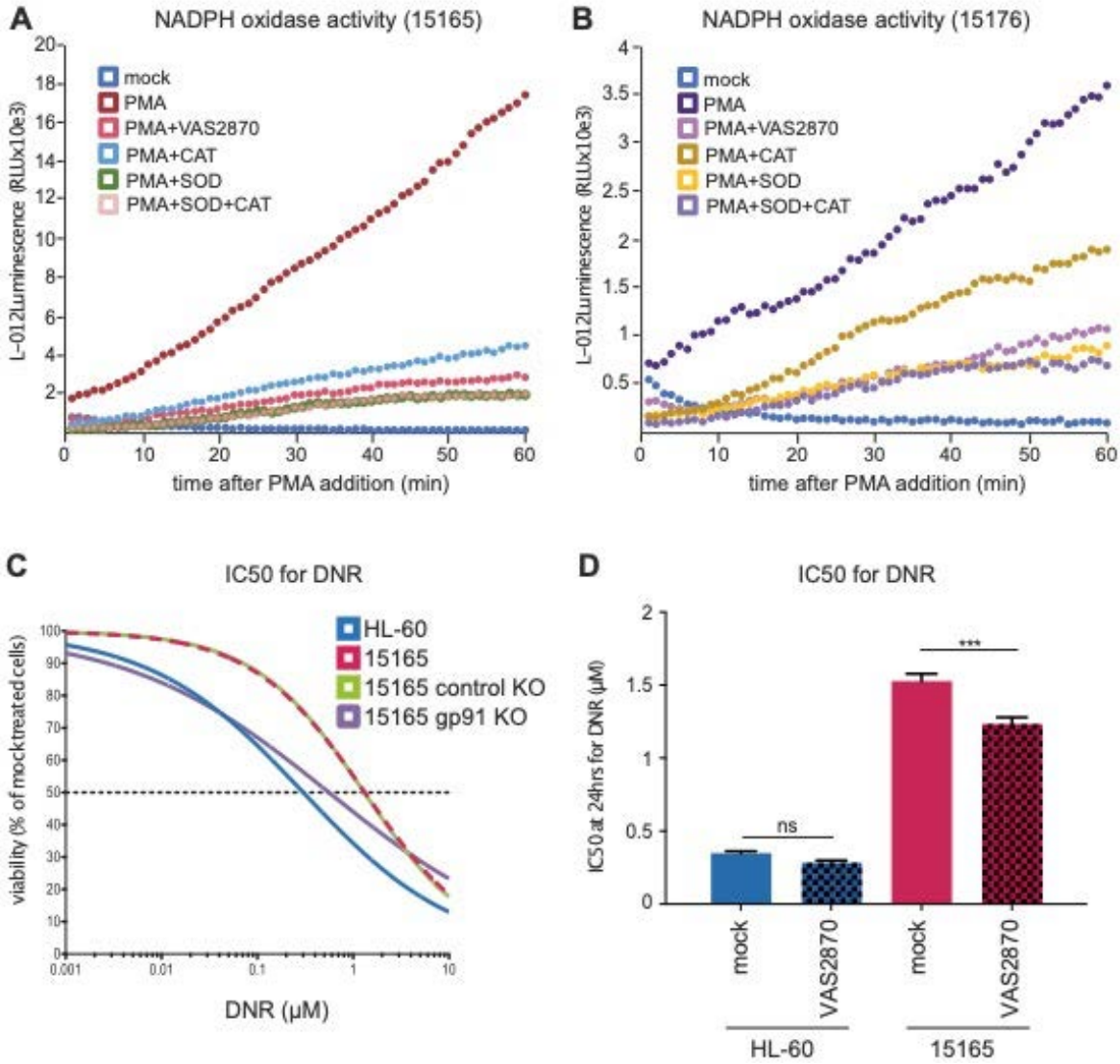

Figure S5. DNR-R clones produce high NOX-derived ROS, which are involved in their resistance to DNR. (A,B) DNR-R clones 15165 (A) and 15176 (B) were stimulated or not with PMA and ROS production was measured by luminometry. When indicated, VAS2870 (10 µM) or SOD (30 U/mL) and/or Catalase (25 µg/mL) were added to the reaction mixture 10 min before PMA addition (n=3, a representative experiment is shown). (C) IC_{50} for DNR was measured after 24 hrs of treatment using MTS (n=4, non-linear fit of all experiments). (D) HL60 and one DNR-R clone (15165) were cultured in the presence of VAS2870 (1µM) for 3 weeks. IC_{50} for DNR was measured after 24 hrs of DNR treatment using MTS (n=4, mean +/- SD). p-values were calculated with One-way Anova and Tukey's multiple comparison test.

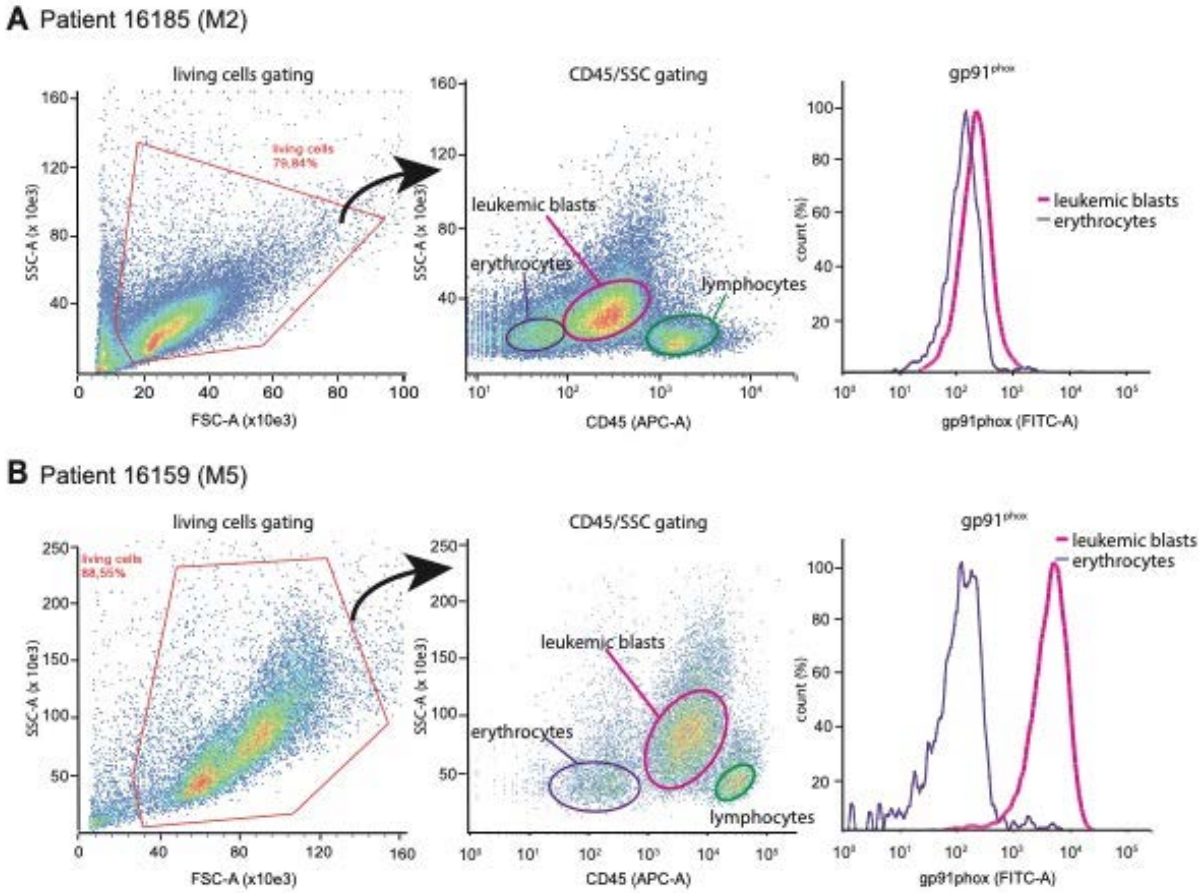

Figure S6: Gating strategy for patient samples. Cells are first distinguished from debris and dead cells using FSC/SSC gating. Using CD45/SSC plot, the leukemic cells are distinguished from other populations present in the sample as $CD45^{dim}/SSC^{low}$. Erythrocytes are $CD45^{neg}/SSC^{low}$ while lymphocytes $CD45^{high}/SSC^{low}$.

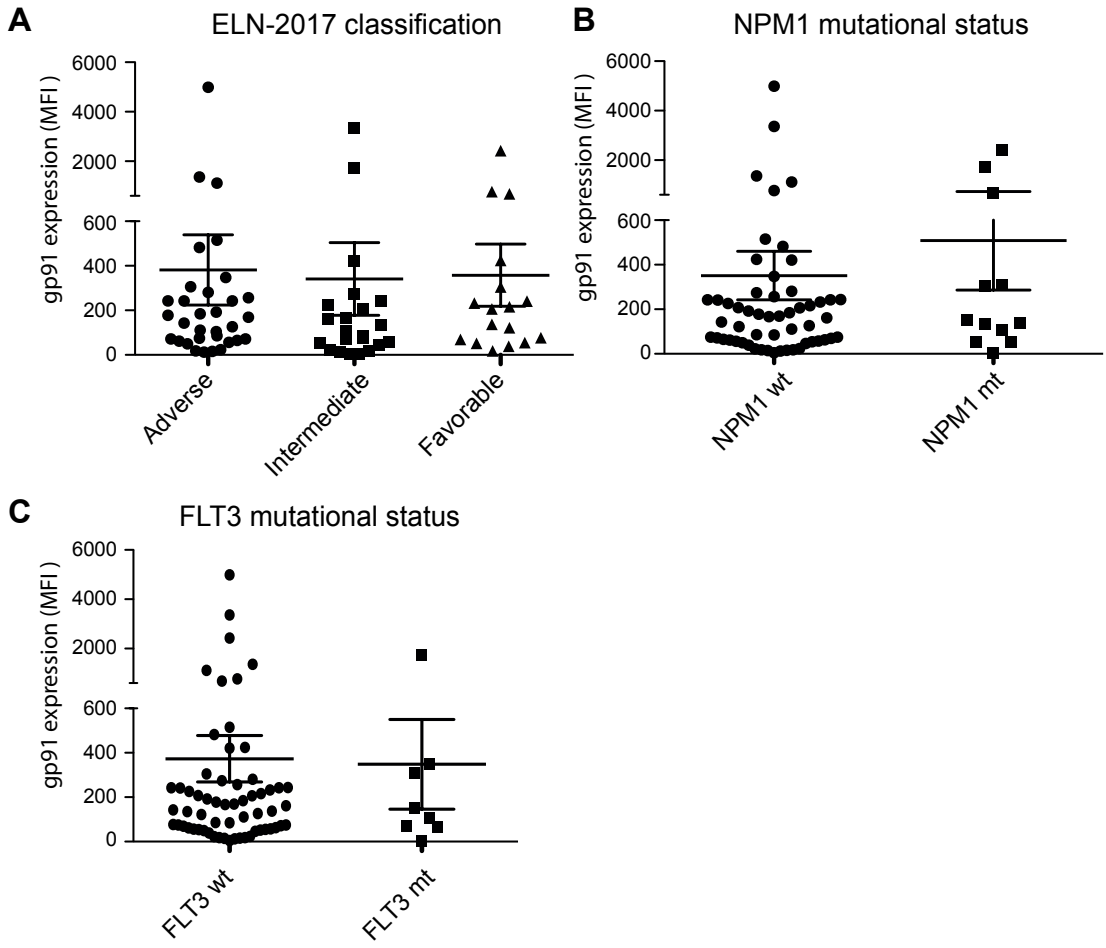

Figure S7: gp91phox expression in AML cells is not correlated with ENL2017 risk classification, NPM1 or FLT3 mutational status. gp91^{phox} expression (MFI) was measured by flow cytometry on bone marrow aspirates from 74 patients taken at diagnosis. Patients are classified according to (A) the ELN-2017 classification, (B) NPM1 mutational status or (C) FLT3 mutational status. No significant differences between groups using Mann-Whitney test.

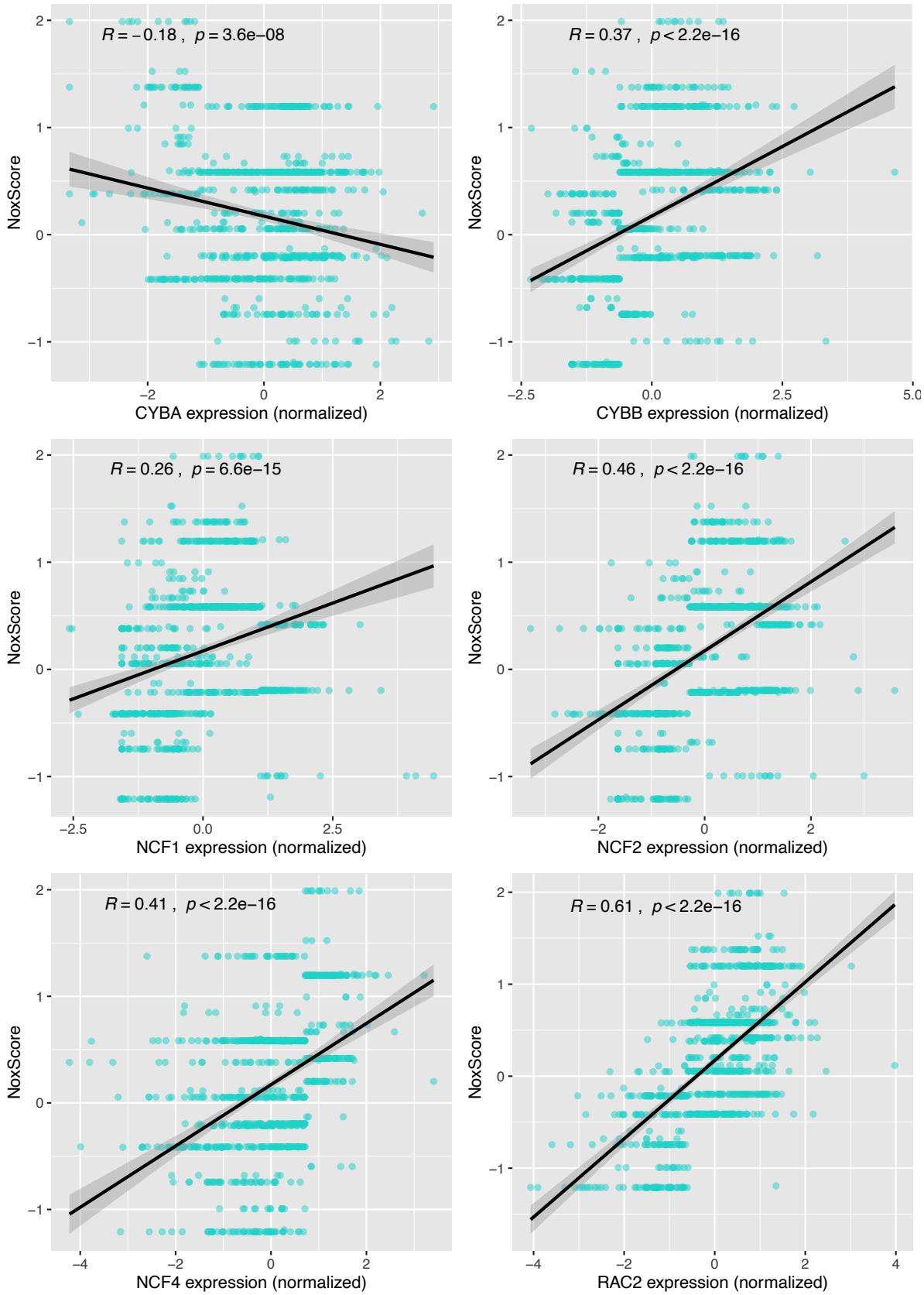

Figure S8: Correlation between the NOX score and the expression of NOX2 genes. The NOX score was plotted as a function of the normalized expression of *CYBA, CYBB, NCF1, NCF2, NCF4* and *RAC2* genes for all patients in the Verhack, Metzeler and TCGA cohorts. Pearson coefficient (R) and associated p-values are indicated.

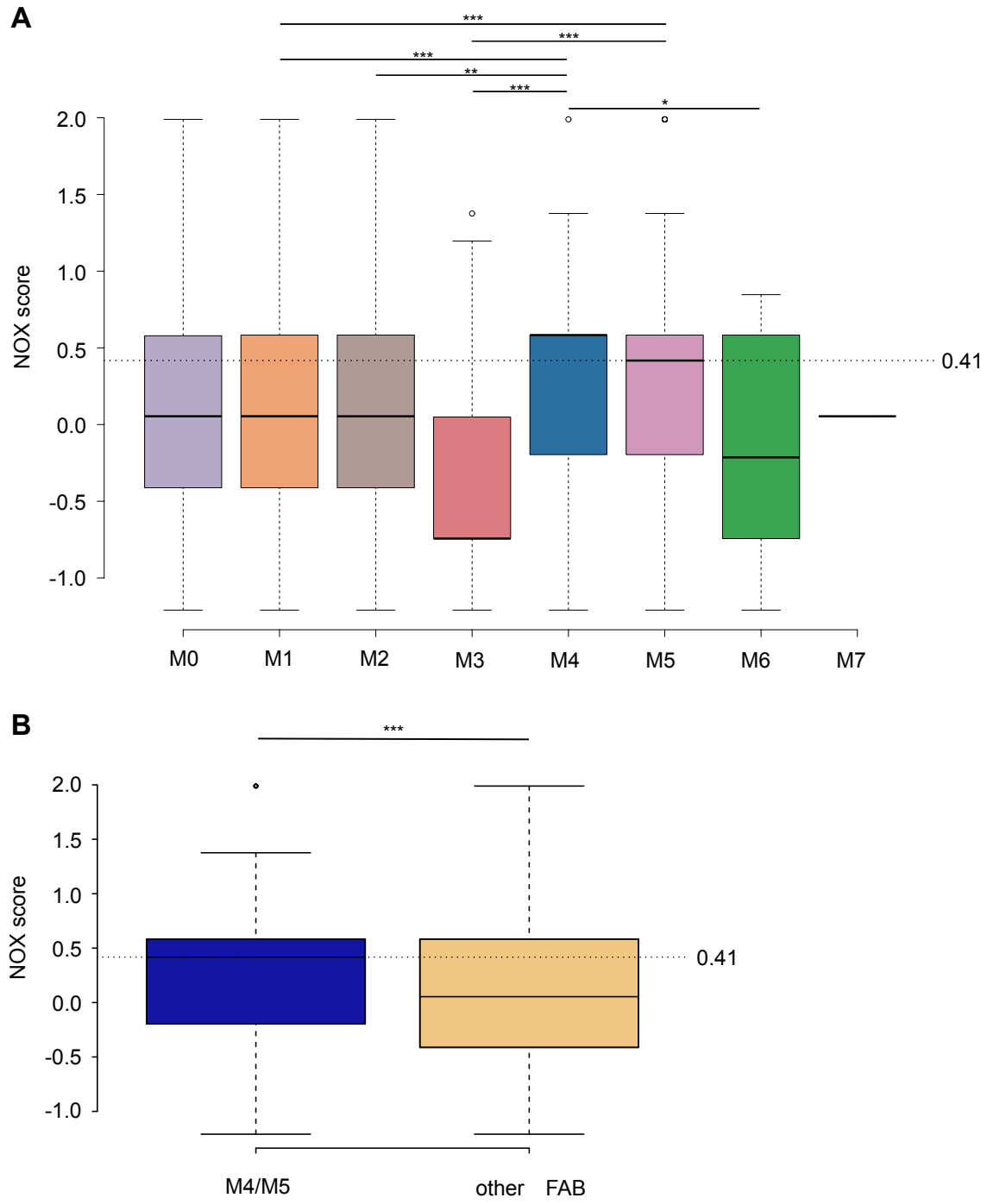

Figure S9: Patients from the FAB M4/M5 subtypes have higher NOX scores. (A) The NOX score was calculated for each FAB subtype using a global cohort comprising all patients from the 3 cohorts (Verhack, Metzeler and TCGA). (B) The NOX score was calculated for M4/M5 and for the other subtypes using the global cohort data. The median NOX scores are indicated as a line and groups were compared using Kruskal-Wallis test (A) and Wilcoxon (B) non parametric tests.

Table S1: Differentially Expressed Genes between DNR-R and ARA-R cells compared to parental HL-60 cells.

Table S2: Ontology analysis of up- and down-regulated genes in DNR-R and ARA-R compared to parental HL-60.

Table S3: Clinical characteristics of the patient included in this study

Table S4: High NOX score gene signature. Mean expression for each Affimetrix probe for all patients from the Verhaak cohort who had a NOX score above 1.37 (10% of patients) was divided by the mean expression for the patients who had a NOX score below 0.41 (50% of patients). The 50 genes having the highest ratio are presented.

Table S5: Prognosis value of the individual NOX genes in the Metzeler cohort. *Gene symbol, adjusted p-value, hazard ratio and prognosis significance are provided for each gene, as determined in the Metzeler cohort (n=240).*

Gene symbol	Hazard ratio	Benjamini Hochberg corrected p-value	Prognosis
CYBA	0,598	0.1013	NS
CYBB	1,479	0.0530	NS
NCF1	0,664	0.0239	Good
NCF2	1,728	0.0397	Poor
NCF4	1,735	0.0122	Poor
RAC2	1,445	0.1050	NS

Table S6: Prognosis value of the individual NOX genes in the TCGA cohort. *Gene symbol, adjusted p-value, hazard ratio and prognosis significance are provided for each gene, as determined in the TCGA cohort (n=148).*

Gene symbol	Hazard ratio	Benjamini Hochberg corrected p-value	Prognosis
CYBA	0,709	0.1107	NS
CYBB	1,281	0.2483	NS
NCF1	2,268	0.0531	NS
NCF2	2,338	0.0048	Poor
NCF4	2,197	0.0047	Poor
RAC2	2,095	0.0009	Poor